



OPEN

Genomic diversifications of five *Gossypium* allopolyploid species and their impact on cotton improvement

Z. Jeffrey Chen^{1,2,14}✉, Avinash Sreedasyam^{3,14}, Atsumi Ando^{1,14}, Qingxin Song^{1,2,14}, Luis M. De Santiago^{4,14}, Amanda M. Hulse-Kemp⁵, Mingquan Ding^{1,6}, Wenxue Ye², Ryan C. Kirkbride¹, Jerry Jenkins³, Christopher Plott³, John Lovell³, Yu-Ming Lin⁴, Robert Vaughn⁴, Bo Liu⁴, Sheron Simpson⁷, Brian E. Scheffler⁷, Li Wen⁸, Christopher A. Sasaki⁸, Corrinne E. Grover⁹, Guanqing Hu⁹, Justin L. Conover⁹, Joseph W. Carlson¹⁰, Shengqiang Shu¹⁰, Lori B. Boston³, Melissa Williams³, Daniel G. Peterson¹¹, Keith McGee¹², Don C. Jones¹³, Jonathan F. Wendel⁹, David M. Stelly⁴, Jane Grimwood³✉ and Jeremy Schmutz^{3,10}

Polyploidy is an evolutionary innovation for many animals and all flowering plants, but its impact on selection and domestication remains elusive. Here we analyze genome evolution and diversification for all five allopolyploid cotton species, including economically important Upland and Pima cottons. Although these polyploid genomes are conserved in gene content and synteny, they have diversified by subgenomic transposon exchanges that equilibrate genome size, evolutionary rate heterogeneities and positive selection between homoeologs within and among lineages. These differential evolutionary trajectories are accompanied by gene-family diversification and homoeolog expression divergence among polyploid lineages. Selection and domestication drive parallel gene expression similarities in fibers of two cultivated cottons, involving coexpression networks and N⁶-methyladenosine RNA modifications. Furthermore, polyploidy induces recombination suppression, which correlates with altered epigenetic landscapes and can be overcome by wild introgression. These genomic insights will empower efforts to manipulate genetic recombination and modify epigenetic landscapes and target genes for crop improvement.

Polyploidy or whole-genome duplication provides genomic opportunities for evolutionary innovations in many animal groups and all flowering plants^{1–5}, including most important crops such as wheat, cotton and canola or oilseed rape^{6–8}. The common occurrence of polyploidy may suggest its advantage and potential for selection and adaptation^{2,3,9}, through rapid genetic and genomic changes as observed in newly formed *Brassica napus*¹⁰, *Tragopogon miscellus*¹¹ and polyploid wheat¹², and/or largely epigenetic modifications as in *Arabidopsis* and cotton polyploids^{5,13}. Cotton is a powerful model for revealing genomic insights into polyploidy³, providing a phylogenetically defined framework of polyploidization (~1.5 million years ago (Ma))¹⁴, followed by natural diversification and crop domestication¹⁵. The evolutionary history of the polyploid cotton clade is longer than that of some other allopolyploids, such as hexaploid wheat (~8,000 years)¹², tetraploid canola (~7,500 years)¹⁶ and tetraploid *Tragopogon* (~150 years)¹¹. Polyploidization between an A-genome African species (*Gossypium arboreum* (Ga)-like) and a D-genome American species (*G. raimondii* (Gr)-like) in the New

World created a new allotetraploid or amphidiploid (AD-genome) cotton clade (Fig. 1a)¹⁴, which has diversified into five polyploid lineages, *G. hirsutum* (Gh) (AD)₁, *G. barbadense* (Gb) (AD)₂, *G. tomentosum* (Gt) (AD)₃, *G. mustelinum* (Gm) (AD)₄ and *G. darwinii* (Gd) (AD)₅. *G. ekmanianum* and *G. stephensii* are recently characterized and closely related to Gh¹⁷. Gh and Gb were separately domesticated from perennial shrubs to become annualized Upland and Pima cottons¹⁵. To date, global cotton production provides income for ~100 million families across ~150 countries, with an annual economic impact of ~US\$500 billion worldwide⁶. However, cotton supply is reduced due to aridification, climate change and pest emergence. Future improvements in cotton and sustainability will involve use of the genomic resources and gene-editing tools becoming available in many crops^{9,18,19}.

Cotton genomes have been sequenced for the D-genome (Gr)²⁰ and A-genome (Ga)²¹ diploids and two cultivated tetraploids^{22–26}. These analyses have shown structural, genetic and gene expression variation related to fiber traits and stress responses in cultivated

¹Department of Molecular Biosciences, The University of Texas at Austin, Austin, TX, USA. ²State Key Laboratory for Crop Genetics and Germplasm Enhancement, Nanjing Agricultural University, Nanjing, China. ³HudsonAlpha Institute for Biotechnology, Huntsville, AL, USA. ⁴Department of Soil and Crop Sciences, Texas A&M University System, College Station, TX, USA. ⁵US Department of Agriculture-Agricultural Research Service, Genomics and Bioinformatics Research Unit, Raleigh, NC, USA. ⁶College of Agriculture and Food Science, Zhejiang A&F University, Lin'an, China. ⁷US Department of Agriculture-Agricultural Research Service, Genomics and Bioinformatics Research Unit, Stoneville, MS, USA. ⁸Department of Plant and Environmental Sciences, Clemson University, Clemson, SC, USA. ⁹Department of Ecology, Evolution, and Organismal Biology, Iowa State University, Ames, IA, USA. ¹⁰The US Department of Energy Joint Genome Institute, Walnut Creek, CA, USA. ¹¹Institute for Genomics, Biocomputing and Biotechnology and Department of Plant and Soil Sciences, Mississippi State University, Mississippi State, MS, USA. ¹²School of Agriculture and Applied Sciences, Alcorn State University, Lorman, MS, USA. ¹³Agriculture and Environmental Research, Cotton Incorporated, Cary, NC, USA. ¹⁴These authors contributed equally: Z. Jeffrey Chen, Avinash Sreedasyam, Atsumi Ando, Qingxin Song, Luis M. De Santiago. ✉e-mail: zjchen@austin.utexas.edu; jgrimwood@hudsonalpha.org

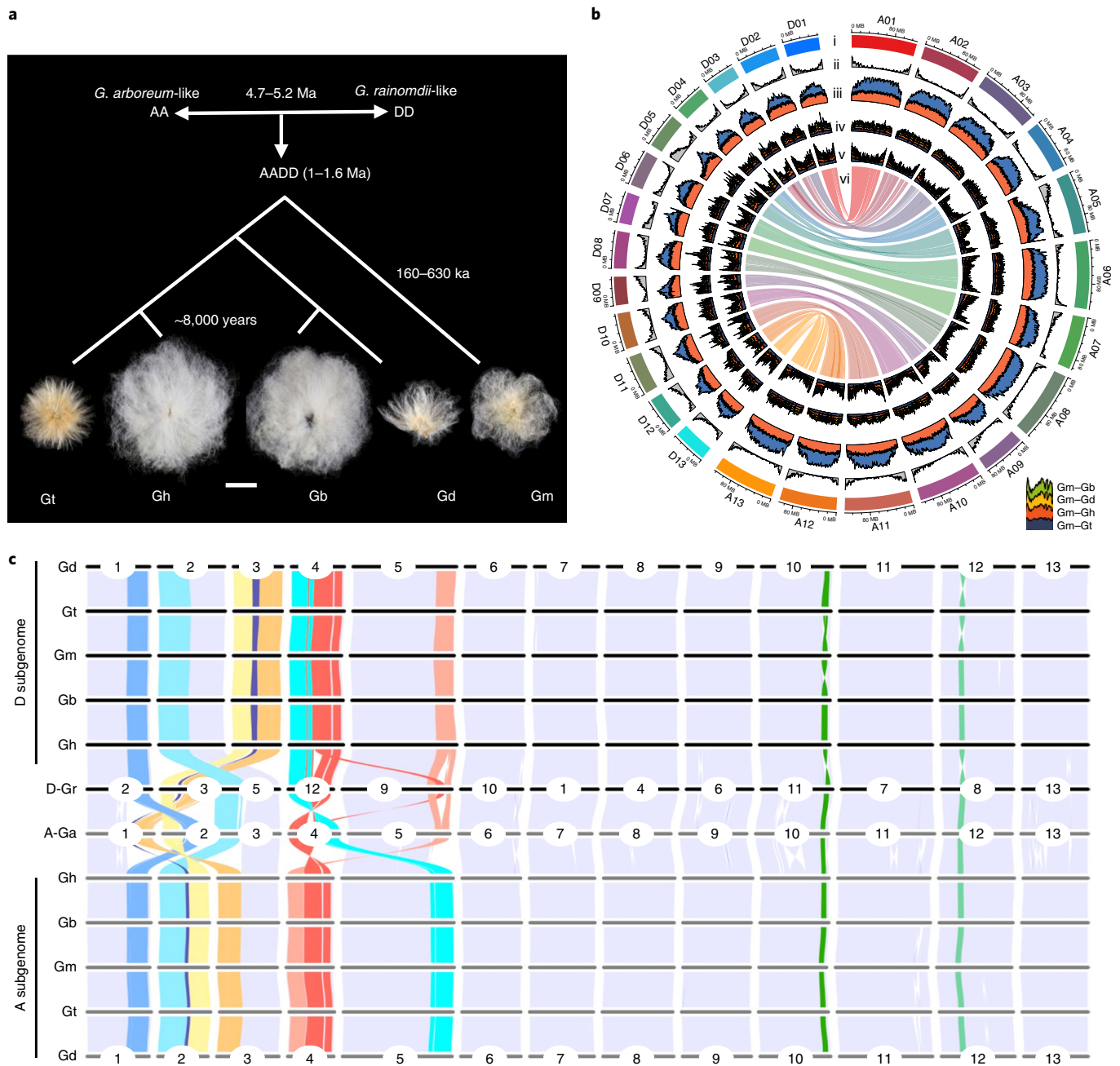


Fig. 1 | Sequencing features of five cotton allotetraploid species. a, Evolution and domestication of five polyploid lineages, Gh, Gb, Gt, Gd and Gm, after polyploidization between an A-genome African species (Ga-like) and a D-genome American species (Gr-like). Typical seeds from each species are shown. The divergence time estimates are based on 21,567 single orthologs among the 5 species by using the synonymous substitution rate (r) of 3.48×10^{-9} (Methods and Supplementary Note). Scale bar, 10 mm; ka, thousand years ago. **b**, Chromosomal features and synteny of the Gm genome. Notes in circles plots: (i) estimated lengths of 13 A and 13 D homoeologous pseudo-chromosomes; (ii) distribution of annotated genes; (iii) TE content (*Gypsy*, steel blue; *Copia*, grey; other repeats, orange); (iv,v) stacked SNP (iv) and indel (v) densities between Gm and Gb, Gd, Gh and Gt, respectively (see inset), and (vi) syntenic blocks between the homoeologous A and D chromosomes. The densities in plots in (ii)–(v) are represented in 1 Mb with overlapping 200-kb sliding windows. **c**, Genome-wide syntenic relationships among A and D subgenomes in five allotetraploids relative to the A-genome-like Ga (A_2 genome) and D-genome-like Gr (D_5 genome). Structural variations among syntenic blocks are marked with colored ribbons.

cottons, but the impact of polyploidy on selection and domestication among the wild and cultivated polyploid cotton species remains poorly understood⁶. Here we report high-quality genomes for all five allotetraploid species and show that despite wide geographic distribution and diversification, allotetraploid cotton genomes retained the syntenic gene content and genomic diversity relative to respective extant diploids. Evolutionary rate heterogeneities, gene

loss and positively selected genes characterize the two subgenomes of each species but differ among polyploid lineages. Transposable elements (TEs) are dynamically exchanged between the two subgenomes, facilitating genome-size equilibration following allopolyploidy. Gene expression diversity in the fiber tissues involves selection, coexpression networks and N^6 -methyladenosine (m^6A) RNA modifications. In cultivated polyploid cottons, recombination

Table 1 | Genome assembly and annotation statistics for five allotetraploid cotton species

Genomic features	Gh	Gb	Gm	Gt	Gd
Estimate of genome size (bp)	2,305,241,538	2,195,804,943	2,315,094,184	2,193,557,323	2,182,957,963
Number of scaffolds	1,025	2,048	383	319	334
Total length of scaffolds (Mb)	2,305.2	2,195.8	2,315.1	2,193.6	2,183.0
Scaffold N50L (Mb)	108.1	93.8	106.8	102.9	101.9
Number of contigs	6,733	4,766	2,147	750	821
Total length of contigs (Mb) and gap (%) ^a	2,302.3 (0.1%)	2,193.9 (0.1%)	2,297.5 (0.8%)	2,189.2 (0.2%)	2,178.1 (0.2%)
Contig N50L (Mb)	0.7839	1.8	2.3	10	9.1
Genome in chromosomes (%)	98.9	97.0	99.0	99.2	99.1
Number of genes	75,376	74,561	74,699	78,338	78,303
Repeat sequences (%)	73.21	72.24	72.85	72.24	72.29

^aA gap is a representation of the assembled sequence with unknown sequence information. bp, base pair; Mb, megabase pairs.

suppression correlates with DNA hypermethylation and weak chromatin interactions and can be overcome by wild introgression and possibly epigenetic remodeling. The results offer unique insights into polyploid genome evolution and provide valuable genomic resources for cotton research and improvement.

Results

Sequencing, assembly and annotation. Sequencing of the five allotetraploid cotton genomes entailed using complementary whole-genome shotgun strategies, including sequencing by single-molecule real-time (PacBio SEQUEL and RSII, ~440× genome equivalent), Illumina (HiSeq and NovaSeq, ~286×) (Supplementary Dataset 1a) and chromatin conformation capture (Hi-C seq) (~326×) (Methods). Homozygous single nucleotide polymorphisms (SNPs) and insertions/deletions (indels) were also used to correct the consensus sequence (Supplementary Dataset 1b,c). The rate of anchored scaffolds is 97% in Gb and 99% or higher in the other 4 species. Scaffolds were oriented, ordered and assembled into 26 pseudo-chromosomes with very low (0.1–0.8%) gaps (Table 1 and Supplementary Dataset 1d). The assembled genomes range in size from 2.2 to 2.3 gigabase pairs (Gbp; Table 1), slightly smaller than the sum of the two A- and D-genome diploids (1.7A + 0.8D ≈ 2.5 Gbp/AD)^{20,21}. Nearly 73% of the assembled genomes are repeats and TEs (Supplementary Dataset 1e), predominantly in pericentromeric regions in Gm (Fig. 1b) and the other 4 species (Extended Data Fig. 1). The completeness and contiguity of these genomes compare favorably with Sanger-based sequences of sorghum²⁷ and *Brachypodium*²⁸.

The euchromatic sequences of 5 polyploid genomes are complete (Supplementary Note), as supported by BUSCO scores (>97%) and 36,880 (>99%) primary transcripts from the Gr version 2 release²⁰ (Supplementary Dataset 1b), with the number of protein-coding genes predicted to range from 74,561 (Gb) to 78,338 (Gt; Table 1), which are 3,000–4,000 more than reported in Gh and Gb²³. Although the A subgenome (1.7 Gbp) is twice the size of the D subgenome (0.8 Gbp)^{20,21}, mirroring the ancestral state of their extant diploids, the two have similar numbers of protein-coding genes (ratio of D/A ≈ 1.06; Supplementary Dataset 1f).

As an indication of the improved contiguity (Supplementary Note), the contig length in the Gh genome increases 6.9-fold with a 7.7-fold reduction in fragmentation (6,733 versus 51,849), compared to the published sequences²². The improvement is substantial in the Gb genome with a 15.9-fold reduction in N50 contigs and a 23-fold increase in N50 contig length (from 77.6 to 1,800 kilobase pairs (kb)). Moreover, most quality scores are 2–5-fold higher in the 3 wild polyploid species than in Gh and Gb (Table 1).

Reciprocal 24-nucleotide masking and syntenic analyses show that our Gh and Gb assemblies have ~23- and 2.7-fold more unique sequences, respectively, than the published ones²² also with variable gap sizes (10–200 kb; Extended Data Fig. 2a). Some specific genes are present in our annotations and the published data, which are largely related to gene copy number variation (more decreases than increases). Other differences include inversions (132–133 megabase pairs (Mb)) with two large ones (A06 and D03) present in similar regions of both Gh and Gb²² (Extended Data Fig. 2b), which could result from errors and/or unresolved alternative haplotypes; these inversions were confirmed using Hi-C data (Extended Data Fig. 2c). Notably, the published Hai7124 strain²² is a Gb local strain that is different from Gb 3-79, and Gh TM-1 strains may vary; these can also contribute to the observed variation.

Evolution within and between five polyploids. Using the diploid^{20,21} and 5 polyploid cotton genomes, we estimated divergence at 58–59 Ma between *Gossypium* and its relative *Theobroma cacao* (Extended Data Fig. 3a and Supplementary Note), 4.7–5.2 Ma between the extant diploids (Extended Data Fig. 3b), and 1.0–1.6 Ma between polyploid and diploid clades. Genome-wide phylogenetic analysis (Extended Data Fig. 4a) supports a monophyletic origin for the five allotetraploid species²⁹. Within the polyploid clade, the highest divergence (~0.63 Ma) occurs between Gm and the other 4 species, with the most recent divergence (~0.20 Ma) between Gb and Gd. This genomic diversification was accompanied by biogeographic radiation to the Galapagos Islands (Gd), the Hawaiian Islands (Gt), South America (northeastern Brazil) (Gm)³⁰, Central and South America, the Caribbean, and the Pacific (Gh and Gb)³¹, with separate distribution and domestication of diploid cultivated cottons in southern Arabia, North Africa, western India and China³² (Extended Data Fig. 4b). Over the last 8,000 years, Upland (Gh) and Pima (Gb) cottons were independently domesticated in northwest South America and the Yucatan Peninsula of Mexico, respectively, under strong human selection, leading to the modern annualized crops¹⁵.

After whole-genome duplication, duplicate genes may be lost or diverge in functions³³, but the pace of this process has rarely been studied in allopolyploids. Using 17,136 homoeolog pairs shared among all 5 allotetraploid species, we demonstrate that most (14,583, 85.5%) homoeolog pairs evolved at statistically indistinguishable rates throughout the polyploid clade relative to the diploids (Supplementary Dataset 2a), but those with rate shifts occur more commonly in the A (1,476, 8.5%) than in the D (845, 5%) subgenome. We further revealed that the D homoeologs generally acquire substitution mutations more quickly than the A homoeologs in most

lineages, whereas the Gh and Gt lineages experience a greater rate of divergence in the A than in the D homoeologs (Supplementary Dataset 2b). This relative acceleration of A-homoeolog divergence is mirrored in lineage-specific rate tests; the Gh/Gt clade including Upland cotton has the fastest evolving A homoeologs and the slowest evolving D homoeologs among five polyploids. These results demonstrate pervasive lineage-specific rate heterogeneities between subgenomes and among different polyploid cottons.

We examined patterns of gene loss and gain using 4,369 single-copy orthologs (SCOs), which are present in both diploids and in one or more allotetraploids (Extended Data Fig. 4c). Analysis of gene loss and gain among these basally shared homoeologs in the five polyploid lineages showed the highest level of net gene loss between the initial polyploidization and Gm, with threefold higher levels in the A subgenome (547 net gene losses) than in the D subgenome (149). Other polyploids have fewer gene losses with no subgenomic bias.

Among the homoeologs shared by all five polyploid species (Fig. 2a), the number of genes under positive selection (K_a/K_e values > 1) is the highest (3,200–3,300) in Gm with the longest branch relative to others, and the lowest between Gb and Gd (~1,100), the most recently diverged polyploid clade (Supplementary Dataset 3). Across different polyploid lineages, 10–20% more D homoeologs are under positive selection than A homoeologs, suggesting a concerted evolutionary impact on subgenomic functions in all polyploid species.

Genomic diversity among five polyploids. The two subgenomes in each of the five polyploid species are highly conserved at the chromosomal, gene content and nucleotide levels (Fig. 1b and Extended Data Fig. 1). The D subgenomes have fewer and smaller inversions than the A subgenomes (Fig. 1c), as reported for Gh²⁵, except for a few small inversions in D10 of Gt–Gm and Gm–Gb and D12 of Gd–Gt–Gm. This level of structural conservation is similar to some polyploids such as wheat⁷ and *Arabidopsis suecica*³⁴, but is different from others such as *B. napus*¹⁰, peanut³⁵ and *T. miscellus*¹¹, which show rapid homoeologous shuffling.

The genomic conservation is extended to gene order, collinearity and synteny (Fig. 1c). Among the annotated genes (74,561–78,338), 56,870 orthologous groups or 65,300 genes (32,650 homoeologous pairs) (84–88%) are shared among all 5 species (Fig. 2a and Supplementary Dataset 1f).

The number of SNPs is in the range of 4–12 million (1.7–5.2 SNPs kb⁻¹) or 0.19–0.53% among 5 polyploid genomes (Supplementary Dataset 4 and Supplementary Note). Gm has the highest SNP level (0.53%) relative to the other 4 species, with the lowest between the most recently diverged species Gb and Gd (~0.19%). Similar trends of indels range from ~5.55 Mb (~0.76%) in Gm–Gt to ~3.35 Mb (~0.34%) in Gb–Gd (Extended Data Fig. 1 and Supplementary Dataset 5). The level of overall variation of SNPs and indels among cotton species is low, comparable to natural variation (3.5–4.1 SNPs kb⁻¹) between *Brachypodium* accessions²⁸ but lower than that (~7.4 SNPs kb⁻¹) for subspecies of rice³⁶. SNPs are more frequent in pericentromeric regions, while indel distributions coincide with gene densities (Fig. 1b and Extended Data Fig. 1).

TE exchanges between two subgenomes that equilibrate the genome-size variation. The size difference between the Ga (~1.7 Gbp) and Gr (~0.8 Gbp)^{20,21} genomes is preserved in the respective A and D subgenomes of the 5 allotetraploid species (Fig. 3a). The A subgenome consists of a substantial amount of repetitive DNA in centromeric and pericentromeric regions (Fig. 3b). However, the A subgenome has 4.0–5.9% lower repetitive DNA content than the A-genome diploid (Ga), whereas the D subgenome has 1.5–2.9% higher content than the D-genome diploid (Gr) in Gh (Fig. 3c) and the other 4 species (Extended Data Fig. 5a).

Consistently, the D subgenome has 10–20% more long terminal repeat (LTR) TEs than the D-genome diploid, while the A subgenome has 3–11% fewer LTRs than the A-genome diploid. These changes in subgenomic TEs may account for slight genome downsizing (Table 1) and genome-size equilibration following allopolyploidy in all five species, suggesting that the ‘evolutionary tape’ is replayed across polyploid lineages.

Copia- and *Gypsy*-like TEs are the most abundant LTRs in the Gh genome²⁵. Estimates indicate that divergence of 5.6% (Gt) to 15.5% (Gh) and 39.7% (Gb) LTRs occurred during polyploid diversification (<0.6 Ma; Extended Data Fig. 5b–f). Since polyploid formation, LTRs increased substantially in the D subgenome of all five polyploids (Fig. 3d). The results indicate activation of LTRs in the D subgenome following polyploidization or movement of LTRs from the A to D subgenome³⁷. Indeed, some *Copia*- and *Gypsy*-like elements are present in the D subgenome but absent in the extant D-genome diploid (Extended Data Fig. 5g).

Gene family diversification. The domesticated (Gh and Gb) and wild (Gm, Gt and Gd) cotton species share 417 (403) and 464 (359) unique genes (orthogroups) in respective groups (Fig. 2a), and no species-specific orthogroups are identified, although they possess distinct phenotypic traits such as fiber length (Fig. 1a) and flower morphology (Fig. 2c,d). The unique genes in the two domesticated cottons are over-represented in biological processes such as microtubule-based movement and lipid biosynthetic process and transport in the domesticated cottons (Fig. 2e; $P < 0.05$), reflecting the traits related to fiber development and cottonseed oil. Moreover, many of these genes are under positive selection and overlap regions of domestication traits including fiber yield and quality in Upland cotton³⁸ (Supplementary Dataset 6). The unique genes in all three wild polyploid species, however, are enriched for pollination and reproduction (Fig. 2f), suggesting a role of these genes in reproductive adaptation in natural environments.

Plants have evolved an intricate innate immune system to protect them from pathogens and pests through intracellular disease-resistance (R) proteins as a defense response³⁹. Among the R genes (Methods and Supplementary Note), each species has its unique R genes with very few genes shared between species (Fig. 2b and Supplementary Dataset 7), despite 5 wild and cultivated species sharing a core R-gene set (271), suggesting extensive diversification of R genes during selection and domestication. This is in contrast to a shared set of unique genes (related to fiber and seed traits) between the two cultivated species and the other shared set (related to reproductive and adaptive traits) among the three wild species (Fig. 2a).

Between the two subgenomes, the D subgenome has higher numbers of R genes (7.8%) than does the A subgenome ($P = 0.0126$, Student's *t*-test; Supplementary Dataset 7). Using the published data⁴⁰, we found expression induction of ~96% of 291 and 384 predicted R genes in the A and D subgenomes, respectively, by bacterial blight pathogens; 19 in D and 7 in A are upregulated at significant levels (error corrected, FDR = 0.05 and $P < 0.001$, exact test), while a similar trend of R-gene expression is observed after the reniform nematode attack (Supplementary Dataset 8), suggesting a contribution of the D-genome species to disease-resistance traits.

Gene expression diversity. In the five allotetraploid species sequenced, gene expression diversity is dynamic and pervasive across developmental stages and between subgenomes (Supplementary Dataset 9). Principal component analysis shows clear separation of expression between developmental stages (PC1) and between subgenomes (PC3; Extended Data Fig. 6a), with more D homoeologs expressed than A homoeologs in most tissues examined (Extended Data Fig. 7), consistent with higher levels of tri-methylation of Lys 4 on histone H3 (H3K4me3) in the former

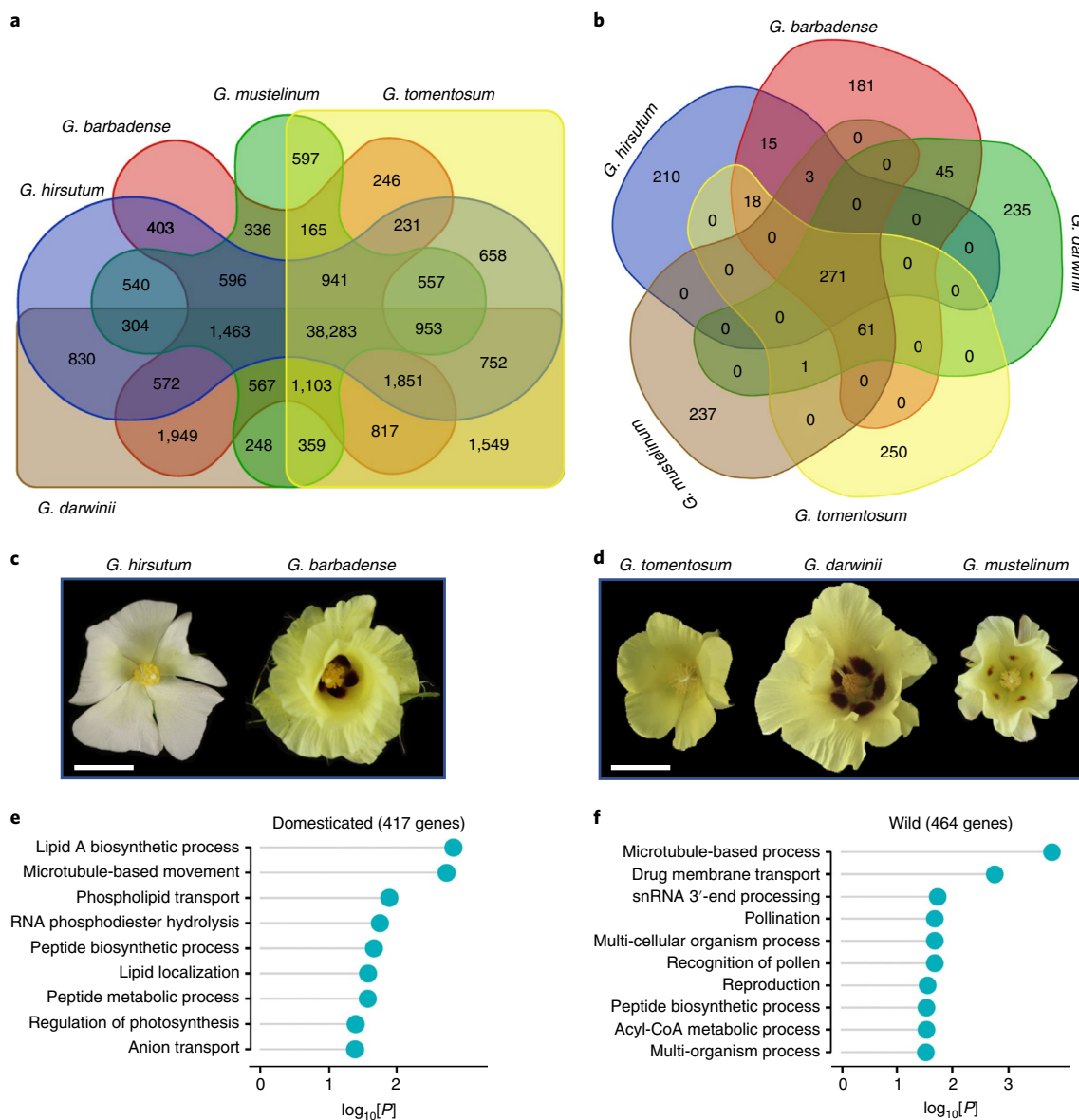


Fig. 2 | Gene family expansion and contraction in cultivated and wild allotetraploid cotton species. a, Venn diagram representing the shared orthologous groups (orthogroups) between cotton species. No species-specific orthogroups were identified by Orthofinder (Methods). **b**, Venn diagram of R-gene family expansion and contraction in these five species. **c,d**, Flower morphology of two cultivated (**c**) and three wild (**d**) polyloid cotton species. Scale bars, 30 mm. **e,f**, Gene Ontology (GO)-term enrichment of the shared genes in polyloid domesticated cottons (**e**) and wild species (**f**).

than in the latter⁴¹. Notably, expression correlates more closely with the subgenomic variation than with tissue types, except for fiber elongation and cellulose biosynthesis, where subgenomic expression patterns are more closely correlated between Upland and Pima cottons (Extended Data Fig. 6b). This may suggest that domestication drives parallel expression similarities of fiber-related genes in the two cultivated species.

These differentially expressed genes in fibers may contribute to fiber development, as they show enrichment of GO groups in hydrolase and GTPase-binding activities (Extended Data Fig. 8a,b). Hydrolases are essential for plant cell wall development⁴², and Ras and Ran GTPases are implicated in the transition from primary to secondary wall synthesis in fibers⁴³. Moreover, translation and ribosome biosynthesis pathway genes are enriched during fiber elongation in Upland cotton and during cellulose biosynthesis in Pima cotton, consistent with faster fiber development in Upland cotton and longer fiber duration in Pima cotton⁴⁴.

Expression networks and m⁶A RNA in fibers. Gene expression diversity is also reflected by coexpression modules in fibers among four species (Supplementary Dataset 10 and Supplementary Note). These module-related genes show higher semantic similarities between domesticated cottons (Gh–Gb) than with two wild species (Gt and Gm). The modules include supramolecular fiber organization genes in Upland cotton and brassinosteroid signaling genes in Pima cotton, which could affect fiber cell elongation⁴⁵. The two wild species have different biological functions and transcription factors enriched in fiber-related gene modules (Supplementary Dataset 11), which may account for the fiber traits that are very different from those of the domesticated species (Fig. 1a).

Transcriptional and post-transcriptional regulation, including the activity of small RNAs and DNA methylation, mediates fiber cell development⁴⁶. Modification of m⁶A messenger RNA can stabilize mRNA and promote translation with a role in developmental regulation of plants and animals⁴⁷. In Upland cotton, m⁶A peaks are

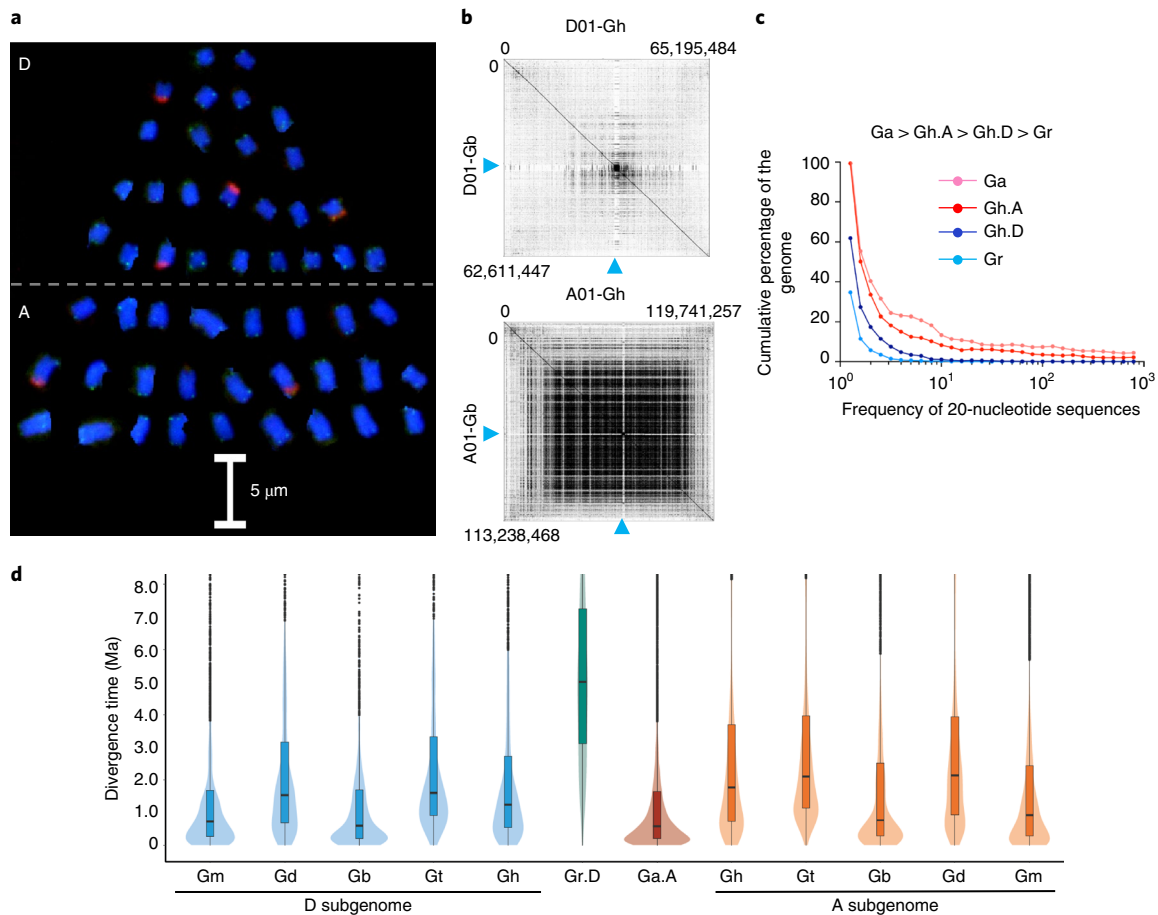


Fig. 3 | Genomic diversification of A and D subgenomes in five allotetraploid cotton species. **a**, Chromosome painting of Gh using DNA probes to label telomeres (green) and 25S ribosomal DNA (red); DNA is stained by 4',6-diamidino-2-phenylindole (DAPI, blue). The A (lower half) and D (upper half) homoeologous chromosomes are separated and rearranged into a tree shape. **b**, Pairwise comparison (dot plots) of 18-nucleotide sequences between the Gh and Gb homoeologous chromosomes D01 (top) and A01 (bottom) using Genome Pair Rapid Dotter (Gepard) plot analysis (Methods). The blue arrowheads indicate approximate centromeric locations. Genomic length positions are shown in each plot. **c**, Cumulative percentages (y axis) of 20-nucleotide sequences and their frequencies (x axis) in the A and D subgenomes of Gh relative to Ga (A) and Gr (D). **d**, The divergence time (Ma) of TEs (*Copia* and *Gypsy*) in the A and D subgenomes relative to their A- and D-genome-like diploids, Ga.A and Gr.D, respectively. The divergence time was estimated using the synonymous substitution rate (r) of 3.48×10^{-9} (Methods and Supplementary Note).

found largely in the 5' and 3' untranscribed regions (Extended Data Fig. 8c) of 1,205 genes in developing fibers (Supplementary Dataset 12), at levels 7-fold more than in leaves (Extended Data Fig. 8d) ($P < 0.002$, Student's t -test), while the number of expressed genes is similar in both tissues. Notably, both m⁶A-modified mRNAs and transcriptome data in the fibers target the genes involved in translation, hydrolase activity and GTPase-binding activities (Extended Data Fig. 8a). These results indicate that mRNA stability and translational activities may determine fiber elongation and cellulose biosynthesis when cell cycles arrest in fiber cells.

Recombination and epigenetic landscapes. Polyploidy leads to low genetic recombination, as observed in *B. napus*⁴⁸, which may comprise bottlenecks for breeding improvement. To determine the recombination landscapes in polyploid cottons, we genotyped 17,134 SNPs using the new Gh sequence and the CottonSNP63K array⁴⁹ and identified a total of 1,739 low-recombination haplotype blocks (cold spots) in Upland cotton using whole-genome population-based linkage analysis⁵⁰ (Methods and Supplementary Note). These blocks (average ~678.9kb with 8.4 SNPs) span 1.18 Gbp (~52%) of the genome, including ~58% and ~41% in the A and D subgenomes, respectively (Fig. 4a), and are dispersed among all chromosomes

with large ones predominately near pericentromeric regions. Recombination is generally suppressed throughout haplotype blocks, in contrast to that in subtelomeric regions (Extended Data Fig. 9a).

Chromosome A08 has 62 haplotype blocks, including an exceptionally large one (~72 Mb) (Fig. 4b). Interestingly, interspecific hybridization between different tetraploids can increase recombination rates in these regions. For example, in the Gb × GhF₂ population, recombination rates increased more than 4–6 cM Mb⁻¹ in the left region (29–30 Mb) and in two other regions in the same Gb × GhF₂ population. Recombination rates were also increased in the Gm × GhBC₁F₁ population (Fig. 4b). Similar increases were observed in the homoeologous D08 low-recombination haplotype blocks in the Gb × GhF₂ population. Moreover, these haplotype blocks of either parent segregated with expected ratios within the population of Gh × GmBC₂F₁ (Extended Data Fig. 9b) or Gh × GtBC₃F₁ (Extended Data Fig. 9c). These data suggest the stability and selection of these haplotype regions during domestication and breeding.

Notably, genome-wide recombination cold spots (haplotype block) and hotspots (no haplotype block) correlated with the DNA methylation frequency at CG, CHG (H = A, T or C) and CHH sites in the cultivated allotetraploids Gh and Gb (Pearson $r = 0.994$; Fig. 4c and Extended Data Fig. 10a,b), with higher methylation

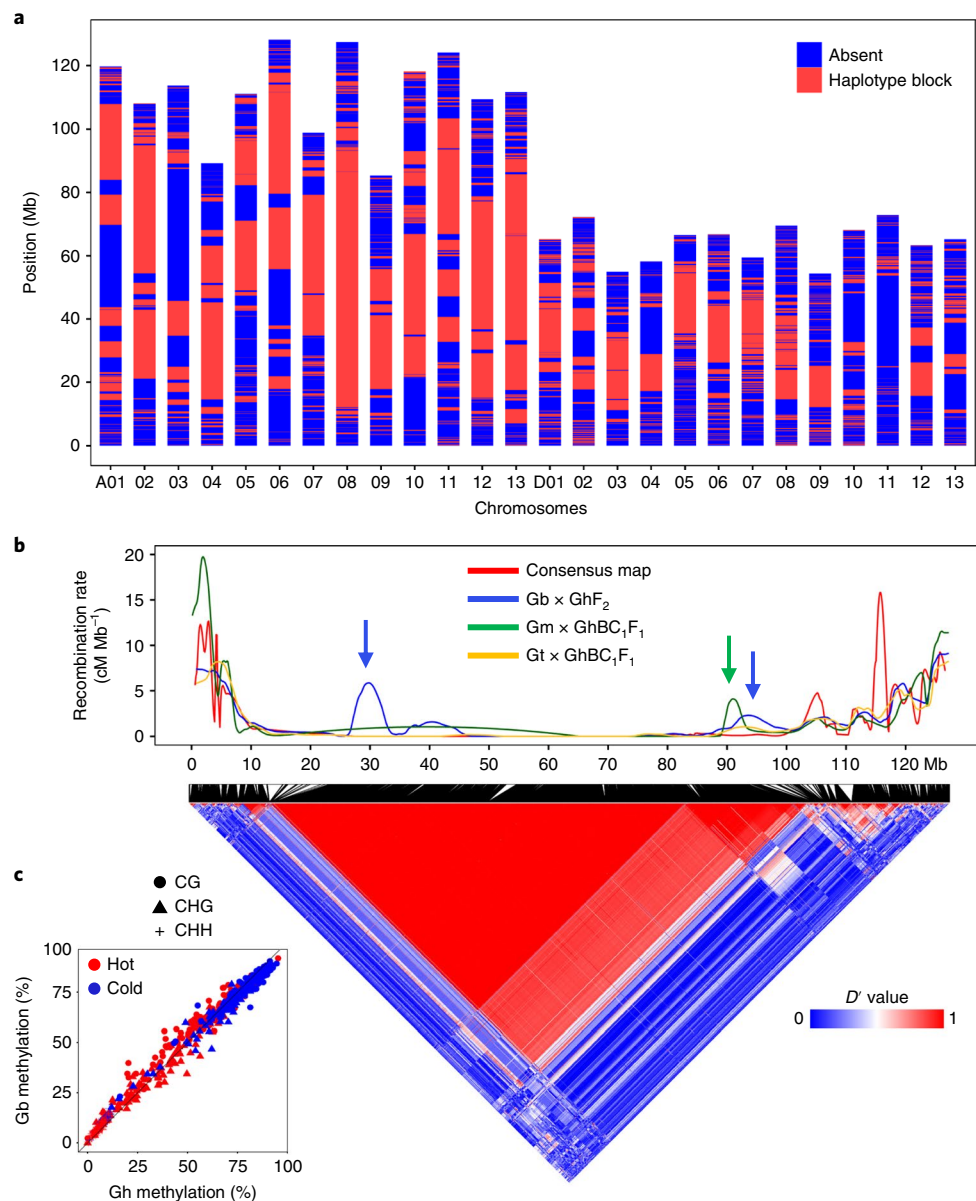


Fig. 4 | Low-recombination haplotype blocks and their stability and selection during breeding and domestication. **a**, Distribution of presence (red) or absence (blue) of low-recombination haplotype blocks (red) in each pseudo-molecule of the A (A01–A13) and D (D01–D13) subgenomes in Gh. Map positions (Mb) are indicated in the y axis. **b**, A low-recombination haplotype block near the pericentromeric region (~72 Mb) of chromosome A08 (bottom). The color indicates the coefficient of linkage disequilibrium (D') from low (blue) to high (red) with the upper confidence bound ($D' = 0.90$) for the recombination cutoff. The recombination rates (y axis; using locally estimated scatterplot smoothing (LOESS) regression, Methods and Supplementary Note) in Gb \times GhF₂ (blue), Gm \times GhBC₁F₁ (green), Gt \times GhBC₁F₁ (yellow) and the consensus (red) are shown above with the positions (Mb, x axis). Two elevated recombination events are detected in Gb \times GhF₂ (blue arrows) and one in Gm \times GhBC₁F₁ (green arrow). **c**, The average percentage (%) of CG (circle), CHG (triangle) and CHH (cross) methylation in the recombination hotspots (red) and cold spots (blue) between Gb and Gh. The CHH methylation is clustered in the left lower corner, which is visible in an enlarged image (Extended Data Fig. 10a).

frequencies in the cold spots than in the hotspots (analysis of variance (ANOVA), $P < 1 \cdot 10^{-6}$). The data support the role of DNA methylation in altering recombination landscapes, as reported in *Arabidopsis*^{51,52}. Consistent with this notion, DNA methylation changes that are induced in the interspecific hybrid (Ga \times Gr) are also largely maintained in the five allotetraploid cotton species, creating hundreds and possibly thousands of epialleles, including the ones responsible for photoperiodic flowering and worldwide cultivation of cotton⁵³.

Moreover, recombination events in all three interspecific crosses (Gb \times GhF₂, Gm \times GhBC₁F₁ and Gt \times GhBC₁F₁) correlated

negatively with the average numbers of strongly connecting sites (intensity > 5) ($P < 8.842 \times 10^{-16}$) and their connection intensities ($P < 7.26 \times 10^{-12}$) of the Hi-C chromatin matrix (Pearson $r = -0.874$; Extended Data Fig. 10c). Recombination hotspots have fewer but more intense chromatin interactions within short distances, while the cold spots tend to have more but weaker interactions in long distances (Extended Data Fig. 10c,d). For example, 2 hotspots and 9 cold spots in the A08 region (Extended Data Fig. 10d), including 7 cold spots spanning ~32 Mb correlated with weak Hi-C intensities and DNA hypermethylation (Extended Data Fig. 10e). These data indicate that DNA hypermethylation and

weak chromatin interactions interfere with recombination events in polyploid cottons.

Discussion

Despite wide geographic distribution and diversification, five allotetraploid cotton genomes have largely retained the gene content and genomic synteny relative to respective extant diploids. This level of genome stability is in contrast to rapid genomic changes observed in some newly formed allotetraploids such as *B. napus*¹⁰ and *T. miscellus*¹¹. However, in cultivated canola, the two subgenomes are relatively undisrupted⁸, probably because the extant parental species existing today to make new tetraploids¹⁰ may be different from the ones that formed cultivated canola ~7,500 years ago¹⁶ and likely became extinct. In addition, all five cotton polyploid species have a monophyletic origin, which is similar to the origin of wild and domesticated tetraploid peanuts⁵⁴, but different from recurrent formation of *Tragopogon* tetraploids⁵⁵. Notably, since polyploid formation 1–1.5 Ma, the evolution of 2 subgenomes in each of the 5 allotetraploid cotton species does not exhibit a simple asymmetrical pattern, as reported in Upland cotton²⁵. Instead, the two subgenomes have diversified and experienced novel heterogeneous evolutionary trajectories, including partial equilibration of subgenome size mediated by differential TE exchanges, pervasive evolutionary rate shifts, and positive selection between homoeologs within and among lineages. These features present in all five allotetraploid species suggest that the ‘evolutionary tape’ is replayed during polyploid diversification and speciation.

Among the five allotetraploid genomes, no species-specific orthologs were identified, except for one set of the unique genes related to fiber and seed traits in the two domesticated cottons and another set of the unique genes for reproduction and adaptation in the three wild polyploid species. However, R-gene families have rapidly evolved in each allotetraploid and extensively diversified during selection and domestication. These genomic diversifications have been accompanied by dynamic and prevalent gene expression changes during growth and development between wild and cultivated polyploid species, including parallel gene expression, coexpression networks and m⁶A mRNA modifications in fibers of the cultivated species. Remarkably, polyploid cotton genomes show recombination suppression or haplotype blocks, which correlate with altered epigenetic landscapes and can be overcome by wild introgression and possibly epigenetic manipulation. This finding is contemporary to the discovery of the *Ph1* locus that inhibits pairing of homoeologous chromosomes in polyploid wheat^{56,57}. The recombination suppression may help maintain a repository of epigenes or epialleles that were generated by interspecific hybridization accompanied by polyploidization and could have shaped polyploid cotton evolution, selection and domestication⁵³. These conceptual advances and genomic and epigenetic resources will help improve cotton fiber yield and quality as a sustainable alternative to petroleum-based synthetic fibers. Modifying epigenetic landscapes and using gene-editing tools may also overcome the limited genetic diversity within polyploid cottons. These principles may facilitate future efforts to concomitantly enhance the economic yield and sustainability of this global crop and possibly other polyploid crops.

Online content

Any methods, additional references, Nature Research reporting summaries, source data, extended data, supplementary information, acknowledgements, peer review information; details of author contributions and competing interests; and statements of data and code availability are available at <https://doi.org/10.1038/s41588-020-0614-5>.

Received: 3 February 2020; Accepted: 16 March 2020;
Published online: 20 April 2020

References

- Muller, H. J. Why polyploidy is rarer in animals than in plants. *Am. Nat.* **59**, 346–353 (1925).
- Soltis, D. E., Visger, C. J. & Soltis, P. S. The polyploidy revolution then... and now: Stebbins revisited. *Am. J. Bot.* **101**, 1057–1078 (2014).
- Wendel, J. F. The wondrous cycles of polyploidy in plants. *Am. J. Bot.* **102**, 1753–1756 (2015).
- Leitch, A. R. & Leitch, I. J. Genomic plasticity and the diversity of polyploid plants. *Science* **320**, 481–483 (2008).
- Chen, Z. J. Genetic and epigenetic mechanisms for gene expression and phenotypic variation in plant polyploids. *Annu. Rev. Plant Biol.* **58**, 377–406 (2007).
- Chen, Z. J. et al. Toward sequencing cotton (*Gossypium*) genomes. *Plant Physiol.* **145**, 1303–1310 (2007).
- International Wheat Genome Sequencing Consortium et al. Shifting the limits in wheat research and breeding using a fully annotated reference genome. *Science* **361**, eaar7191 (2018).
- Chalhoub, B. et al. Early allopolyploid evolution in the post-Neolithic *Brassica napus* oilseed genome. *Science* **345**, 950–953 (2014).
- Bevan, M. W. et al. Genomic innovation for crop improvement. *Nature* **543**, 346–354 (2017).
- Xiong, Z., Gaeta, R. T. & Pires, J. C. Homoeologous shuffling and chromosome compensation maintain genome balance in resynthesized allopolyploid *Brassica napus*. *Proc. Natl Acad. Sci. USA* **108**, 7908–7913 (2011).
- Chester, M. et al. Extensive chromosomal variation in a recently formed natural allopolyploid species, *Tragopogon miscellus* (Asteraceae). *Proc. Natl Acad. Sci. USA* **109**, 1176–1181 (2012).
- Feldman, M. et al. Rapid elimination of low-copy DNA sequences in polyploid wheat: a possible mechanism for differentiation of homoeologous chromosomes. *Genetics* **147**, 1381–1387 (1997).
- Ding, M. & Chen, Z. J. Epigenetic perspectives on the evolution and domestication of polyploid plants and crops. *Curr. Opin. Plant Biol.* **42**, 37–48 (2018).
- Wendel, J. F. & Grover, C. E. In *Cotton* 2nd edn (eds Fang, D. D. & Percey, R. G.), Vol. 57, 25–44 (Agronomy Monograph 57, 2015).
- Splitstoser, J. C., Dillehay, T. D., Wouters, J. & Claro, A. Early pre-Hispanic use of indigo blue in Peru. *Sci. Adv.* **2**, e1501623 (2016).
- Lu, K. et al. Whole-genome resequencing reveals *Brassica napus* origin and genetic loci involved in its improvement. *Nat. Commun.* **10**, 1154 (2019).
- Grover, C. E. et al. Re-evaluating the phylogeny of allopolyploid *Gossypium* L. *Mol. Phylogenet. Evol.* **92**, 45–52 (2015).
- Bailey-Serres, J., Parker, J. E., Ainsworth, E. A., Oldroyd, G. E. D. & Schroeder, J. I. Genetic strategies for improving crop yields. *Nature* **575**, 109–118 (2019).
- Eshed, Y. & Lippman, Z. B. Revolutions in agriculture chart a course for targeted breeding of old and new crops. *Science* **366**, eaax0025 (2019).
- Paterson, A. H. et al. Repeated polyploidization of *Gossypium* genomes and the evolution of spinnable cotton fibres. *Nature* **492**, 423–427 (2012).
- Li, F. et al. Genome sequence of the cultivated cotton *Gossypium arboreum*. *Nat. Genet.* **46**, 567–572 (2014).
- Hu, Y. et al. *Gossypium barbadense* and *Gossypium hirsutum* genomes provide insights into the origin and evolution of allotetraploid cotton. *Nat. Genet.* **51**, 739–748 (2019).
- Wang, M. et al. Reference genome sequences of two cultivated allotetraploid cottons, *Gossypium hirsutum* and *Gossypium barbadense*. *Nat. Genet.* **51**, 224–229 (2019).
- Li, F. et al. Genome sequence of cultivated Upland cotton (*Gossypium hirsutum* TM-1) provides insights into genome evolution. *Nat. Biotechnol.* **33**, 524–530 (2015).
- Zhang, T. et al. Sequencing of allotetraploid cotton (*Gossypium hirsutum* L. acc. TM-1) provides a resource for fiber improvement. *Nat. Biotechnol.* **33**, 531–537 (2015).
- Liu, X. et al. *Gossypium barbadense* genome sequence provides insight into the evolution of extra-long staple fiber and specialized metabolites. *Sci. Rep.* **5**, 14139 (2015).
- Paterson, A. H. et al. The *Sorghum bicolor* genome and the diversification of grasses. *Nature* **457**, 551–556 (2009).
- Gordon, S. P. et al. Extensive gene content variation in the *Brachypodium distachyon* pan-genome correlates with population structure. *Nat. Commun.* **8**, 2184 (2017).
- Grover, C. E., Grupp, K. K., Wanzek, R. J. & Wendel, J. F. Assessing the monophyly of polyploid *Gossypium* species. *Plant Syst. Evol.* **298**, 1177–1183 (2012).
- Wendel, J. F., Brubaker, C., Alvarez, I., Cronn, R. & Stewart, J. M. in *Genetics and Genomics of Cotton. Plant Genetics and Genomics: Crops and Models* Vol. 3 (ed. Paterson, A. H.) 3–22 (Springer, 2009).
- Brubaker, C. L., Bourland, F. M. & Wendel, J. F. in *Cotton: Origin, History, Technology, and Production* (eds Smith, C. W. & Cothren, J. T.) 3–32 (John Wiley & Sons, 1999).

32. Kulkarni, V. N., Khadi, B. M., Maralappanavar, M. S., Deshapande L. A. & Narayanan, S. S. in *Genetics and Genomics of Cotton. Plant Genetics and Genomics: Crops and Models* Vol. 3 (ed. Paterson, A. H.) 69–97 (Springer, 2009).
33. Lynch, M. & Conery, J. S. The evolutionary fate and consequences of duplicate genes. *Science* **290**, 1151–1155 (2000).
34. Novikova, P. Y. et al. Genome sequencing reveals the origin of the allotetraploid *Arabidopsis suecica*. *Mol. Biol. Evol.* **34**, 957–968 (2017).
35. Bertoli, D. J. et al. The genome sequence of segmental allotetraploid peanut *Arachis hypogaea*. *Nat. Genet.* **51**, 877–884 (2019).
36. Zhang, J. et al. Extensive sequence divergence between the reference genomes of two elite *indica* rice varieties Zhenshan 97 and Minghui 63. *Proc. Natl Acad. Sci. USA* **113**, E5163–E5171 (2016).
37. Zhao, X. P. et al. Dispersed repetitive DNA has spread to new genomes since polyploid formation in cotton. *Genome Res.* **8**, 479–492 (1998).
38. Ma, Z. et al. Resequencing a core collection of upland cotton identifies genomic variation and loci influencing fiber quality and yield. *Nat. Genet.* **50**, 803–813 (2018).
39. Jones, J. D. & Dangl, J. L. The plant immune system. *Nature* **444**, 323–329 (2006).
40. Phillips, A. Z. et al. Genomics-enabled analysis of the emergent disease cotton bacterial blight. *PLoS Genet.* **13**, e1007003 (2017).
41. Zheng, D. et al. Histone modifications define expression bias of homoeologous genomes in allotetraploid cotton. *Plant Physiol.* **172**, 1760–1771 (2016).
42. Schroder, R., Atkinson, R. G. & Redgwell, R. J. Re-interpreting the role of endo-beta-mannanases as mannan endotransglycosylase/hydrolases in the plant cell wall. *Ann. Bot.* **104**, 197–204 (2009).
43. Trainin, T., Shmuel, M. & Delmer, D. P. In vitro prenylation of the small GTPase Rac13 of cotton. *Plant Physiol.* **112**, 1491–1497 (1996).
44. Tuttle, J. R. et al. Metabolomic and transcriptomic insights into how cotton fiber transitions to secondary wall synthesis, represses lignification, and prolongs elongation. *BMC Genomics* **16**, 477 (2015).
45. Sun, Y. et al. Brassinosteroid regulates fiber development on cultured cotton ovules. *Plant Cell Physiol.* **46**, 1384–1391 (2005).
46. Song, Q., Guan, X. & Chen, Z. J. Dynamic roles for small RNAs and DNA methylation during ovule and fiber development in allotetraploid cotton. *PLoS Genet.* **11**, e1005724 (2015).
47. Shen, L., Liang, Z., Wong, C. E. & Yu, H. Messenger RNA modifications in plants. *Trends Plant Sci.* **24**, 328–341 (2019).
48. Cifuentes, M. et al. Repeated polyploidy drove different levels of crossover suppression between homoeologous chromosomes in *Brassica napus* allohaploids. *Plant Cell* **22**, 2265–2276 (2010).
49. Hinze, L. L. et al. Diversity analysis of cotton (*Gossypium hirsutum* L.) germplasm using the CottonSNP63K Array. *BMC Plant Biol.* **17**, 37 (2017).
50. Purcell, S. et al. PLINK: a tool set for whole-genome association and population-based linkage analyses. *Am. J. Hum. Genet.* **81**, 559–575 (2007).
51. Mirouze, M. et al. Loss of DNA methylation affects the recombination landscape in *Arabidopsis*. *Proc. Natl Acad. Sci. USA* **109**, 5880–5885 (2012).
52. Yelina, N. E. et al. DNA methylation epigenetically silences crossover hot spots and controls chromosomal domains of meiotic recombination in *Arabidopsis*. *Genes Dev.* **29**, 2183–2202 (2015).
53. Song, Q., Zhang, T., Stelly, D. M. & Chen, Z. J. Epigenomic and functional analyses reveal roles of epialleles in the loss of photoperiod sensitivity during domestication of allotetraploid cottons. *Genome Biol.* **18**, 99 (2017).
54. Yin, D. et al. Comparison of *Arachis monticola* with diploid and cultivated tetraploid genomes reveals asymmetric subgenome evolution and improvement of peanut. *Adv. Sci.* **7**, 1901672 (2020).
55. Soltis, D. E. & Soltis, P. S. Polyploidy: recurrent formation and genome evolution. *Trends Ecol. Evol.* **14**, 348–352 (1999).
56. Riley, R. & Chapman, V. Genetic control of cytologically diploid behaviour of hexaploid wheat. *Nature* **182**, 713–715 (1958).
57. Griffiths, S. et al. Molecular characterization of Ph1 as a major chromosome pairing locus in polyploid wheat. *Nature* **439**, 749–752 (2006).

Publisher's note Springer Nature remains neutral with regard to jurisdictional claims in published maps and institutional affiliations.



Open Access This article is licensed under a Creative Commons Attribution 4.0 International License, which permits use, sharing, adaptation, distribution and reproduction in any medium or format, as long as you give appropriate credit to the original author(s) and the source, provide a link to the Creative Commons license, and indicate if changes were made. The images or other third party material in this article are included in the article's Creative Commons license, unless indicated otherwise in a credit line to the material. If material is not included in the article's Creative Commons license and your intended use is not permitted by statutory regulation or exceeds the permitted use, you will need to obtain permission directly from the copyright holder. To view a copy of this license, visit <http://creativecommons.org/licenses/by/4.0/>.

© The Author(s) 2020

Methods

Plant materials. *G. hirsutum* L. acc. TM-1 (1008001.06), *G. barbadense* L. acc. 3-79 (1400233.01), *G. tomentosum* L. (7179.01,02,03), *G. darwinii* L. (AD5-32, no. 1808015.09) and *G. mustelinum* L. (1408120.09, 1408120.10, 1408121.01, 1408121.02, 1408121.03) were grown in a greenhouse in College Station at Texas A&M University. Young leaves were collected for preparation of high-molecular-weight DNA using a published method⁵⁸. Total RNA was extracted from leaf, root, stem, square, cotyledon, hypocotyl, meristem, petal, stamen, exocarp, ovule (0, 3, 7, 14, 21 and 35 days post anthesis (DPA)) and fiber (7, 14, 21 and 35 DPA) tissues in Gh; from leaf, root, stem, square, cotyledon, flower, ovule (14 DPA) and fiber (14 DPA) tissues in Gb; from leaf, root, stem, square, cotyledon and fiber (14 DPA) tissues in Gm; from leaf, root, stem, square, flower, ovule (0, 7, 14, 21 and 28 DPA) and fiber (7, 14, 21 and 28 DPA) tissues in Gt; and from leaf, root and stem tissues in Gd. Two or three biological replicates were used for RNA-seq and m⁶A RNA-seq analyses.

Genome sequencing and assembly. Sequencing reads were collected using Illumina HiSeq and NovaSeq and PacBio SEQUEL and RSII platforms. We sequenced and assembled five *Gossypium* genomes using high-coverage (>74×) single-molecule real-time long-read sequencing (Pac Biosciences). A total of six Illumina libraries were sequenced using the HiSeq platform, and two libraries were sequenced using NovaSeq. Initially, all five species were assembled using MECAT⁵⁹ and subsequently polished using long reads, as well as Illumina reads. Gb and Gh were polished using QUIVER⁶⁰, while Gd, Gt and Gm were polished using ARROW⁶⁰. Ten Hi-C libraries were sequenced for five cotton genomes (two for each species). The total amount of Illumina sequenced for all 5 species (Supplementary Dataset 1) is 4,361,212,302 reads for a total of 286.4× of high-quality Illumina bases. A total of 105,182,984 PacBio reads were sequenced for all 5 genomes with a total coverage of 439.61×.

Chromosome integration of Gb and Gh leveraged a combination of published Gh synteny and Hi-C scaffolding. A total of 148,239 unique, non-repetitive, non-overlapping 1-kb sequences were extracted from the published Gh genome²⁵ and aligned to the Gh and Gb MECAT assemblies. Misjoins in the MECAT assembly were identified, and the assembly was scaffolded with Hi-C data using the JUICER pipeline⁶¹. Small rearrangements to both genomes were made using the JUICEBOX interface⁶². Finally, a set of 5,275 clones (474.3 Mb total sequence) were used to patch remaining gaps in the Gh assembly. A total of 626 gaps were patched resulting in 1,871,050 base pairs (bp) being added to the assembly. Gd and Gm were integrated into chromosomes using Gb (3-79) synteny, whereas Gt was integrated using the Gh release assembly version 1 https://phytozome.jgi.doe.gov/pz/portal.html#!info?alias=Org_Ghirsutum_er. Final refinements to the Gt assembly were made using the JUICER/JUICEBOX pipeline⁶¹. In all five of the assemblies, care was taken to ensure that the telomere was properly oriented in the chromosomes, and the resulting sequence was screened for retained vector and/or contaminants. Genome annotation and gene prediction procedures are provided in the Supplementary Note.

Dot plots (pairwise comparisons) were generated using Gepard version 1.30 (ref. ⁶³). The input data consist of 2 FASTA files, as well as the appropriate flags (-seq1 FASTA_FILE_1 -seq2 FASTA_FILE_2 -matrix edna.mat -zoom 65000 -word 18 -lower 0 -upper 20 -greyscale 0 -format png), with the -zoom flag from 65,000 (D subgenome) to 119,000 (A subgenome). The edna.mat file is part of the Gepard version 1.30 release. As a rule of thumb, this factor is generated by dividing the number of bases of the input FASTA file by 1,000. The output from the Gepard command is a PNG image file.

Procedures for the analysis of SNPs and indels are provided in the Supplementary Note.

Comparative analysis with published assemblies. *Assessment of genome completeness.* We evaluated the genome assembly completeness by k-mer masking (24-nucleotide) reciprocally between Gh (TM-1)²² and Gh (TM-1, this study) and between Gb (Hai7124)²² and Gb (3-79, this study). The unmasked contiguous sequences of the unshared sequence were extracted into a FASTA file and analyzed using FASTA statistics. BBMap (<https://sourceforge.net/projects/bbmap/>) and Custom Python scripts (Supplementary Note) were used for this analysis.

Genome comparisons using Hi-C data. The Hi-C libraries IKCF (Gh) and ILDE (Gb) were aligned to published Gh and Gb reference genomes using BWA-MEM⁶⁴. Heatmaps were generated using the JUICER-pre command, and visualized using JUICEBOX⁶². Inversions and rearrangements were further identified using JUICEBOX.

Analysis of chromosomal collinearity, structural rearrangements and gene family composition between reference assemblies. Published Gh and Gb assemblies²² were aligned to the assemblies generated in this study using Minimap2 (ref. ⁶⁵) with the parameter setting '-ax asm5 --eqx'. The resulting alignments were used to identify structural rearrangements and local variations using SyR1⁶⁶. The gene copy numbers and gene families between assemblies were identified using OrthoFinder⁶⁷ based on all annotated protein-coding sequences.

Analysis of evolutionary rate changes and gene gain and loss. *Evolutionary rate changes in subgenomes of allopolyploid cotton during diversification.* Rates of evolution for each subgenome of each species across the phylogeny were calculated using pairwise p-distances for the same 17,136 orthologs in all 5 polyploid species (Extended Data Fig. 4a). The distribution of p-distances between each species was compared for both subgenomes using a one-tailed Wilcoxon signed rank test and Bonferroni correction for multiple testing. Differences in evolutionary rates between the subgenomes within each species were evaluated using a modified relative rate test whereby p-distance distributions were compared for both subgenomes to determine which had the greater p-distance (that is, higher inferred rate). Differences in subgenome evolutionary rates among lineages were estimated using a modified relative rate test that again used the Wilcoxon signed rank test with the p-distances of 17,136 genes, here comparing p-distances between two species relative to an outgroup species. This test was repeated for all possible pairs of tip and outgroup combinations. We also summed the total number of differences contained within all orthologs between each pairwise set of species, excluding all sites in which any of the orthologs contained a gap sequence (Supplementary Dataset 2a). Chi-square tests were used to determine the significance of these total substitution counts (Supplementary Dataset 2b).

Analysis of gene loss and gain after polyploid cotton formation. A total of 32,622 groups of SCO groups were identified between subgenomes of all 5 allopolyploids and the diploids Gr and Ga (Extended Data Fig. 4c). Of those, the 4,369 SCO groups that were present in both diploid species but absent in at least 1 allopolyploid subgenome were evaluated for gene losses specific to allopolyploids. The list of SCO groups was converted into a binary matrix of gene occurrence and mapped onto the inferred phylogeny of ten allopolyploid subgenomes (with five taxa each in the At- and Dt-subgenome clades, rooted by the respective diploid progenitors). Using a likelihood-based mixture model assuming predominantly gene losses over gains and stochastic mapping implemented in GLOOME⁶⁸, both the total number of gene gains and losses per branch and the associated probability of each event across the phylogeny were estimated.

Identification of homoeologs under selection. The homoeolog pairs of five species were used for estimating non-synonymous/synonymous (K_a/K_s) values. Every pair of the sequences were aligned using the MUSCLE alignment software⁶⁹ and then transferred to the AXT format for identifying positively selected genes ($K_a/K_s > 1$) using the KaKs calculator⁷⁰. Positively selected genes in A and D homoeologs were compared pairwise among 5 species (Supplementary Dataset 2).

Analyses of repetitive sequences and TEs. Pairwise comparison of 18-nucleotide sequences between homoeologous chromosomes was performed by Gepard plots⁶³. Analysis of the k-mer content of all of the genomes was conducted by LTR-harvest⁷¹ according to the manual. The whole-genome sequences were suffixed first and then indexed using the seed length 20. The frequency of individual 20-nucleotide sequences was estimated using in-house Perl scripts. This analysis was applied to the two diploid cotton species, Ga and Gr, and the five tetraploid allopolyploids, with the A or D subgenome examined separately. The software LTR-harvest⁷¹ and LTR-finder⁷² was used for identifying full-length LTR retrotransposons. The identification parameters were as follows. For LTR-harvest: overlaps best -seed 20 -minlenltr 100 -maxlenltr 2000 -mindistltr 3000 -maxdistltr 25000 -similar 85 -mintsd 4 -maxtsd 20 -motif tgca -motifm1 1 -vic 60 -xdrop 5 -mat 2 -mis -2 -ins -3 -del -3. For LTR-finder: -D 15000 -d 1000 -L 7000 -l 100 -p 20 -C -M 0.9. The two datasets were integrated to remove false positives using the LTR-retriever packages⁷³. The insertion time was estimated using the formula $T = K_d/2r$, where K_d is the divergence rate and r (3.48×10^{-9}) is the substitution rate in cotton¹⁷.

Full-length TE sequences were extracted from each of the seven species and were used to build a TE database; the cd-hit software⁷⁴ was applied to remove redundancies through self-sequence similarity tests, and sequences with identity > 90% were grouped into the same cluster. A cluster present in only one species was defined as a species-specific TE cluster, and those present in more than one species were considered shared TE clusters. A total of 98,794 full-length LTRs were identified in all 7 cotton species and grouped into 20,583 clusters for analysis of their origins in Ga, Gr, and the A and D subgenomes in 5 allotetraploids.

R-gene family and expression analysis in response to pathogen treatments. We detected nucleotide-binding site, leucine-rich repeat (NBS-LRR) motifs with the pfamscan tool⁷⁵ that uses the hidden Markov model search tool (HMMER) version 3.2.1 (ref. ⁷⁶) by searching primary protein-coding transcripts of each of the 5 allotetraploid cottons against the raw hidden Markov model for the NB-ARC-domain family downloaded from Pfam (PF00931). Identified NBS-LRR protein-coding genes for each of the allotetraploid cottons were further analyzed for amino-terminal (TIR/coiled-coil/other) and other functional domains by searching them against the Pfam-A hidden Markov model with the PfamScan tool and HMMER version 3.1 (ref. ⁷⁶) with default settings (Supplementary Note). Short-read sequencing data for bacterial blight were downloaded from the Sequence Read Archive from the NCBI Bioproject accession PRJNA395458 (ref. ⁴⁹). Reniform nematode sequence data were downloaded from the NCBI Bioproject

accession PRJNA269348. Sequence data were aligned to the 653 predicted R genes from the Gh version 2.0 (this study) with Bowtie2 version 2.3.4.1 and filtered for true-pair alignments. Fragments per kilobase million (FPKM) and read counts per million were determined with RSEM version 1.3.0. Differentially expressed R genes were determined with edgeR⁷⁷ using false discovery rate (FDR)-corrected *P* values of 0.05. Of the 291 A-subgenome and 384 D-subgenome predicted R genes, we found FPKM expression profiles (>1) for at least 1 condition in 281 and 372 of the A- and D-subgenome predicted R genes, respectively. Similarly, in response to reniform nematode challenge in Gh, 274 of 291 A-subgenome and 370 of 384 D-subgenome predicted R genes were expressed at the FPKM level (>1) for at least 1 of the 4 conditions tested.

RNA-seq library construction, sequencing and data normalization. Total RNA was extracted from leaf, root, stem, square, flower, ovule and fiber samples from Gh, Gb, Gt, Gm and Gd species (2 replicates each for 124 samples; Supplementary Dataset 9), using PureLink Plant RNA Reagent (ThermoFisher). After DNase treatment, RNA-seq libraries were constructed using an NEBNext Ultra II RNA Library Kit (NEB), and 150-bp paired-end sequences were generated using an Illumina HiSeq 2500.

Paired-end sequence data were quality trimmed ($Q \geq 25$) and reads shorter than 50 bp after trimming were discarded. Sequences were then aligned to respective allotetraploid cotton genomes and counts of reads uniquely mapping to annotated genes were obtained using STAR (version 2.5.3a). Outliers among the biological replicates were verified on the basis of the Pearson correlation coefficient, $r^2 \geq 0.85$. Fragments per kilobase of exon per million (FPKM) fragments mapped values were calculated for each gene by normalizing the read count data to both the length of the gene and the total number of mapped reads in the sample and considered as the metric for estimating gene expression levels⁷⁸. Normalized count data were obtained using the relative logarithm expression (RLE) method in DESeq2 (version 1.14.1)⁷⁹. Genes with low expression were filtered out, by requiring ≥ 2 RLE-normalized counts in at least 2 samples for each gene. Additional data for RNA-seq expression in fiber (28DAP) tissue in both Gh and Gb were downloaded from the published data⁴⁴ and processed as described above and in the Supplementary Note.

Statistical analysis of differentially expressed genes. To measure the gene expression differences between homoeologous genes in RNA-seq data, we used the DESeq2 package in R based on the negative binomial distribution (Supplementary Note). Only genes with $\log_2[\text{fold change}] \geq 1$, Benjamini–Hochberg-adjusted $P < 0.05$ were retained. The comparison of highly expressed homoeologous gene pairs between subgenomes in different tissues was carried out using a binomial test ($P < 0.05$). GO enrichment was analyzed using topGO⁸⁰, an R Bioconductor package with Fisher's exact test; only GO terms with $P < 0.05$ (FDR < 0.05) were considered significant.

Principal component analysis and correlation coefficient analysis. To visualize subgenome and tissue expression relatedness, we used categorized gene expression values. These expression values were averaged across replicates and log₂-transformed. Principal component analysis employed singular value decomposition via the prcomp function in R⁸¹. Categorized gene expression values were used in this analysis. Pearson's correlation coefficients were determined and hierarchical clustering was carried out using the Euclidian distance and complete linkage method.

m⁶A RNA-seq data analysis. m⁶A RNA-seq libraries were constructed using a modified protocol as previously described⁸². Briefly, total RNA was extracted from young leaf and fiber tissues at 7 DPA (2 replicates each) from Gh by using PureLink Plant RNA Reagent (ThermoFisher). mRNA was collected from total RNA by the Oligotex mRNA mini kit (QIAGEN), fragmented and pulled down using an m⁶A antibody, followed by library construction using the NEBNext Ultra II RNA Library Kit (NEB) without polyA tail selection. Fragmented mRNA-seq libraries (control; input) and m⁶A RNA-seq libraries (IP) were sequenced using an Illumina HiSeq 2500 and 150-bp reads. Illumina reads were mapped to the Gh genome using Tophat 2.1.1 (ref. ⁸³), and the uniquely mapped reads were used to identify m⁶A peaks with the Bioconductor package exomePeak⁸⁴ (Supplementary Dataset 12).

GO terms were extracted from the GeneAnnotation_info.txt file. Identified m⁶A peak genes were analyzed by the Bioconductor package topGO⁸⁰ to identify significantly over-represented GO terms ($P < 0.0001$). The location of RNA (5'UTR, CDS or 3'UTR) for each m⁶A RNA-seq read (both input and IP) was identified using the intersect function of Bedtools⁸⁵. Single, double and triple asterisks indicate statistical significance levels of $P < 0.05$, $P < 0.01$ and $P < 0.001$, respectively (Student's *t*-test).

We extracted the gene expression data for Gh leaf and fiber at 7 DPA corresponding to m⁶A peak genes. 'All' refers to the expression level of all identified homoeologous genes in the leaf and fiber samples, while 'peak' corresponds to the expression level of the identified m⁶A peaks for the genes in leaf (161 genes) and fiber (1,205 genes) samples. Single, double and triple asterisks indicate statistical significance levels of $P < 0.05$, $P < 0.01$ and $P < 0.001$, respectively (Student's *t*-test).

Fluorescence in situ hybridization of A and D homoeologous chromosomes.

Procedures for the preparation of metaphase chromosomes in Gh and fluorescence in situ hybridization were adopted from a published protocol⁸⁶, with a modification that the cotton root tips were pretreated with cycloheximide (25 ppm) for 3 h at room temperature. The 25S rDNA fragment was obtained from *Arabidopsis*⁸⁷ and originally provided by R. Hasterok from Poland. Synthetic oligonucleotides for forward and reverse plant telomeric sequences were PCR-amplified and products were labeled by nick translation to create probe to detect telomeres⁸⁸.

Genotyping and recombination rate analyses. Genotyping data representing an improved cotton panel of 257 Gh accessions were acquired from a previously published diversity analysis⁴⁹ utilizing the CottonSNP63K array⁸⁹. The genotyping data in 2 segregating populations included 18 lines each representing 1 family of a Gh × GmBC₃F₁ population and 33 lines each representing 1 family of a Gh × GtBC₃F₁ population. SNPs with a minor allele frequency greater than 5% and that had less than 10% missing data were retained. Genotyping data were further filtered for homeo-SNPs that occur due to intragenomic sequence identity⁸⁹. Array ID sequences were aligned to the Joint Genome Institute Gh version 2.0 sequence assembly using BLASTn⁹⁰ (version 2.7.1+) with a minimum e-value cutoff of 1×10^{-10} . Homoeologous alignments were corrected for using previously published SNP segregation data^{89,91}, as well as interspecific, bi-parental linkage mapping populations from their respective Gh × GmBC₃F₁ and Gh × GtBC₃F₁ initial mapping populations. Genotyping data were then imputed and phased using Beagle (version 4.1)⁹², and genotypes were converted to ABH format to distinguish genotypic parentage.

It is notable that erroneous SNP calling is a common problem in polyploids and especially in the AD-genome allotetraploid cotton because of homoeologous and paralogous sequences. This issue has been addressed through several methods^{89,93,94}. In this study, we used the published method⁸⁹ to avoid erroneous genotype calling and to provide accurate chromosome-specific and homoeologous haplotype structure. Furthermore, we used a historical estimation of recombination⁹⁵, as shown in the haplotype structure using confidence intervals, as well as in two segregating populations, which led to the accurate estimates of recombination rates between parental alleles using linkage disequilibrium analysis⁹⁵. The haplotype block partitioning was conducted with PLINK⁵⁰ (Supplementary Note).

The recombination map for chromosome A08 of Gh was developed using 4 SNP-based genetic maps, including 3 of interspecific crosses between Gb × Gh (F₂, $n = 195$), Gt × Gh (BC₃F₁, $n = 85$) and Gm × Gh (BC₃F₁, $n = 59$) and 1 consensus map that was generated using 3 intraspecific populations⁹¹. All genetic maps were aligned to the Joint Genome Institute Gh version 2.0 sequence assembly using the previously stated methods. Recombination map visualization was estimated using the R package MareyMap⁹⁶ using the nonlinear LOESS method⁹⁷, and the number of surrounding markers used to fit a local polynomial was 7.5% of the total number of markers per chromosome. Final map plotting was conducted using the R package ggplot2 (ref. ⁹⁸). Localized recombination rates for chromosomes A08 and D08 were estimated using a 1-Mb non-overlapping sliding window with a minimum of 4 SNPs per window as a linear regression threshold using MareyMap.

DNA methylation analysis. Methylome sequencing data were downloaded from a published report⁵³. In brief, methylC-seq reads of all allopolyploid cottons were mapped to genome sequences of Gh and Gb, respectively, using Bismark with the parameters (--score_min L,0,-0.2 -X 1000 --no-mixed --no-discordant)⁹⁹. Only the uniquely mapped reads were retained and used for further analysis. Reads mapped to the same site were collapsed into a single consensus molecule to reduce clonal bias. Cytosine counts were combined into 1,000-bp windows using methylKit 1.2.4 (ref. ¹⁰⁰).

The DNA methylation (CG, CHG and CHH) levels (percentage of methylated cytosines) and average Hi-C seq statistics (number of connections, intensity or interaction matrix, and distance) in each recombination spot were compared using custom Python scripts. The Pearson correlation coefficient (*r*) was estimated using singular value decomposition via the prcomp function in R⁸¹. Single, double and triple asterisks indicate statistical significance levels of $P < 0.001$, $P < 1 \times 10^{-5}$ and $P < 1 \times 10^{-10}$, respectively, using one-way ANOVA.

Chromatin conformation capture (Hi-C) sequencing analysis. Hi-C seq libraries were constructed using a previously described protocol^{101,102}, with modifications. Briefly, young leaves from Gh, Gb, Gt, Gm and Gd (2 replicates each) and fiber samples from Gh were fixed in 1% formaldehyde, and nuclei were extracted. Fixed chromatin was digested with DpnII, filled in using biotin-14-dATP and ligated. The biotin-labeled DNA was extracted and pulled down to construct HiC-seq libraries. Sequencing of Hi-C seq libraries was performed using an Illumina HiSeq 2500 and 150-bp reads. Reads were mapped to respective genomes and analyzed by HiC-Pro¹⁰³. The Hi-C read coverage is 205× for Gh, 45× for Gb, 36× for Gm, 22× for Gd and 17× for Gt. The Hi-C data were largely used to correct orientations and misalignments in the assemblies of contigs and scaffolds. For Gh, Hi-C data were used to generate chromatin connection heatmaps with the HiCPlotter (<https://github.com/kcakdemir/HiCPlotter>). Single, double and triple asterisks indicate

statistical significance levels of $P < 0.001$, $P < 1 \times 10^{-5}$ and $P < 1 \times 10^{-10}$, respectively, using one-way ANOVA.

Reporting Summary. Further information on research design is available in the Nature Genetics Research Reporting Summary linked to this article.

Data availability

Sequencing data are accessible under NCBI BioProject numbers (PRJNA515894 for Gh, PRJNA516412 for Gt, PRJNA516411 for Gb, PRJNA516409 for Gd and PRJNA525892 for Gm). All datasets generated and/or analyzed in this study are available in the Article, the Source Data files that accompany Figs. 1–4 and Extended Data Figs. 1–10, Supplementary Datasets 1–12, the Reporting Summary or the Supplementary Note. Additional data such as raw image files that support this study are available from the corresponding authors upon request.

References

58. Saski, C. A. et al. Sub genome anchored physical frameworks of the allotetraploid Upland cotton (*Gossypium hirsutum* L.) genome, and an approach toward reference-grade assemblies of polyploids. *Sci. Rep.* **7**, 15274 (2017).
59. Xiao, C. L. et al. MECAT: fast mapping, error correction, and de novo assembly for single-molecule sequencing reads. *Nat. Methods* **14**, 1072–1074 (2017).
60. Chin, C. S. et al. Nonhybrid, finished microbial genome assemblies from long-read SMRT sequencing data. *Nat. Methods* **10**, 563–569 (2013).
61. Durand, N. C. et al. Juicebox provides a visualization system for Hi-C contact maps with unlimited zoom. *Cell Syst.* **3**, 99–101 (2016).
62. Robinson, J. T. et al. Juicebox.js provides a cloud-based visualization system for Hi-C data. *Cell Syst.* **6**, 256–258.E1 (2018).
63. Krumsiek, J., Arnold, R. & Rattei, T. Gepard: a rapid and sensitive tool for creating dotplots on genome scale. *Bioinformatics* **23**, 1026–1028 (2007).
64. Li, H. Aligning sequence reads, clone sequences and assembly contigs with BWA-MEM. Preprint at <https://arxiv.org/abs/1303.3997> (2013).
65. Li, H. Minimap2: pairwise alignment for nucleotide sequences. *Bioinformatics* **34**, 3094–3100 (2018).
66. Goel, M., Sun, H., Jiao, W.-B. & Schneeberger, K. Identification of syntenic and rearranged regions from whole-genome assemblies. Preprint at [bioRxiv](https://doi.org/10.1101/546622) <https://doi.org/10.1101/546622> (2019).
67. Emms, D. M. & Kelly, S. OrthoFinder: solving fundamental biases in whole genome comparisons dramatically improves orthogroup inference accuracy. *Genome Biol.* **16**, 157 (2015).
68. Cohen, O. & Pupko, T. Inference of gain and loss events from phyletic patterns using stochastic mapping and maximum parsimony—a simulation study. *Genome Biol. Evol.* **3**, 1265–1275 (2011).
69. Edgar, R. C. MUSCLE: multiple sequence alignment with high accuracy and high throughput. *Nucleic Acids Res.* **32**, 1792–1797 (2004).
70. Wang, D., Zhang, Y., Zhang, Z., Zhu, J. & Yu, J. KaKs_Calculator 2.0: a toolkit incorporating gamma-series methods and sliding window strategies. *Genomics Proteomics Bioinformatics* **8**, 77–80 (2010).
71. Ellinghaus, D., Kurtz, S. & Willhoeft, U. LTRharvest, an efficient and flexible software for de novo detection of LTR retrotransposons. *BMC Bioinformatics* **9**, 18 (2008).
72. Xu, Z. & Wang, H. LTR_FINDER: an efficient tool for the prediction of full-length LTR retrotransposons. *Nucleic Acids Res.* **35**, W265–W268 (2007).
73. Ou, S. & Jiang, N. LTR_retriever: a highly accurate and sensitive program for identification of long terminal repeat retrotransposons. *Plant Physiol.* **176**, 1410–1422 (2018).
74. Li, W. & Godzik, A. Cd-hit: a fast program for clustering and comparing large sets of protein or nucleotide sequences. *Bioinformatics* **22**, 1658–1659 (2006).
75. Chojnacki, S., Cowley, A., Lee, J., Foix, A. & Lopez, R. Programmatic access to bioinformatics tools from EMBL-EBI update: 2017. *Nucleic Acids Res.* **45**, W550–W553 (2017).
76. Eddy, S. R. Accelerated profile HMM searches. *PLoS Comput. Biol.* **7**, e1002195 (2011).
77. Robinson, M. D., McCarthy, D. J. & Smyth, G. K. edgeR: a Bioconductor package for differential expression analysis of digital gene expression data. *Bioinformatics* **26**, 139–140 (2010).
78. Trapnell, C. et al. Differential gene and transcript expression analysis of RNA-seq experiments with TopHat and Cufflinks. *Nat. Protoc.* **7**, 562–578 (2012).
79. Love, M. I., Huber, W. & Anders, S. Moderated estimation of fold change and dispersion for RNA-seq data with DESeq2. *Genome Biol.* **15**, 550 (2014).
80. Alexa, A. & Rahenfuhrer, J. topGO: Enrichment analysis for Gene Ontology. R package version 2.32.0 (2016).
81. R: *A Language and Environment for Statistical Computing* (R Foundation for Statistical Computing, 2018).
82. Dominissini, D., Moshitch-Moshkovitz, S., Salmon-Divon, M., Amariglio, N. & Rechavi, G. Transcriptome-wide mapping of N^6 -methyladenosine by m^6A -seq based on immunocapturing and massively parallel sequencing. *Nat. Protoc.* **8**, 176–189 (2013).
83. Kim, D. et al. TopHat2: accurate alignment of transcriptomes in the presence of insertions, deletions and gene fusions. *Genome Biol.* **14**, R36 (2013).
84. Meng, J., Cui, X. D., Rao, M. K., Chen, Y. D. & Huang, Y. F. Exome-based analysis for RNA epigenome sequencing data. *Bioinformatics* **29**, 1565–1567 (2013).
85. Quinlan, A. R. & Hall, I. M. BEDTools: a flexible suite of utilities for comparing genomic features. *Bioinformatics* **26**, 841–842 (2010).
86. Liu, B. & Davis, T. M. Conservation and loss of ribosomal RNA gene sites in diploid and polyploid *Fragaria* (Rosaceae). *BMC Plant Biol.* **11**, 157 (2011).
87. Unfried, I. & Gruendler, P. Nucleotide sequence of the 5.8S and 25S rRNA genes and of the internal transcribed spacers from *Arabidopsis thaliana*. *Nucleic Acids Res.* **18**, 4011 (1990).
88. Cox, A. V. et al. Comparison of plant telomere locations using a PCR-generated synthetic probe. *Ann. Bot.* **72**, 239–247 (1993).
89. Hulse-Kemp, A. M. et al. Development of a 63K SNP array for cotton and high-density mapping of intraspecific and interspecific populations of *Gossypium* spp. *Genes Genomes Genet.* **5**, 1187–1209 (2015).
90. Camacho, C. et al. BLAST plus: architecture and applications. *BMC Bioinformatics* **10**, 421 (2009).
91. Ulloa, M., Hulse-Kemp, A. M., De Santiago, L. M., Stelly, D. M. & Burke, J. J. Insights into upland cotton (*Gossypium hirsutum* L.) genetic recombination based on 3 high-density single-nucleotide polymorphism and a consensus map developed independently with common parents. *Genomics Insights* **10**, 1–15 (2017).
92. Browning, S. R. & Browning, B. L. Rapid and accurate haplotype phasing and missing-data inference for whole-genome association studies by use of localized haplotype clustering. *Am. J. Hum. Genet.* **81**, 1084–1097 (2007).
93. Korani, W., Clevenger, J. P., Chu, Y. & Ozias-Akins, P. Machine learning as an effective method for identifying true single nucleotide polymorphisms in polyploid plants. *Plant Genome* **12**, 180023 (2019).
94. Clevenger, J. P., Korani, W., Ozias-Akins, P. & Jackson, S. Haplotype-based genotyping in polyploids. *Front. Plant Sci.* **9**, 564 (2018).
95. Gabriel, S. B. et al. The structure of haplotype blocks in the human genome. *Science* **296**, 2225–2229 (2002).
96. Rezvoy, C., Charif, D., Gueguen, L. & Marais, G. A. B. MareyMap: an R-based tool with graphical interface for estimating recombination rates. *Bioinformatics* **23**, 2188–2189 (2007).
97. Cleveland, W. S. & Grosse, E. Computational methods for local regression. *Stat. Comput.* **1**, 47–62 (1991).
98. Wickham, H. *ggplot2: Elegant Graphics for Data Analysis* (Springer, 2009).
99. Krueger, F. & Andrews, S. R. Bismark: a flexible aligner and methylation caller for Bisulfite-Seq applications. *Bioinformatics* **27**, 1571–1572 (2011).
100. Akalin, A. et al. methylKit: a comprehensive R package for the analysis of genome-wide DNA methylation profiles. *Genome Biol.* **13**, R87 (2012).
101. Belton, J. M. et al. Hi-C: a comprehensive technique to capture the conformation of genomes. *Methods* **58**, 268–276 (2012).
102. Louwers, M., Splinter, E., van Driel, R., de Laat, W. & Stam, M. Studying physical chromatin interactions in plants using chromosome conformation capture (3C). *Nat. Protoc.* **4**, 1216–1229 (2009).
103. Servant, N. et al. HiC-Pro: an optimized and flexible pipeline for Hi-C data processing. *Genome Biol.* **16**, 259 (2015).

Acknowledgements

We thank J. R. Ecker, E. S. Dennis, T. Zhang, A. H. Paterson, R. G. Cantrell and C. L. Brubaker for their roles in coordinating the sequencing white paper and J. A. Udall for initial discussion of the cotton diversity project. We also thank Texas Advanced Computing Center, Iowa State University Research Information Technology Unit and the Bioinformatics Center at Nanjing Agricultural University for computational support and assistance. This work is supported by grants from the National Science Foundation (IOS1444552 and IOS1739092 to Z.J.C., IOS1826544 to J.F.W.), the US Department of Agriculture (6066-21310-005-00-D to B.E.S., NACA 58-6066-6-046 and NACA 58-6066-6-059 to D.G.P.) and Cotton Incorporated (14-371 to Z. J.C., 13-965 to J.S., 18-195 to J.F.W., 13-466TX, 13-636, 13-694 and 18-201 to D.M.S.). The work conducted by the US Department of Energy Joint Genome Institute is supported by the Office of Science of the US Department of Energy under contract no. DE-AC02-05CH11231 (S.Shu and J.W.C.). The work is also supported by grants from the National Natural Science Foundation of China (91631302 to Q.S. and Z.J.C.), Jiangsu Collaborative Innovation Center for Modern Crop Production (Q.S. and W.Y.) and the Natural Science Foundation of Zhejiang Province, China (LY17C060005 to M.D.).

Author contributions

Z.J.C., J.G., D.M.S., B.E.S. and C.A.S. conceived and designed the project, A.S., A.A., Q.S., L.M.D.S., A.M.H.-K., M.D., J.J., R.C.K., Y.-M.L., C.P., J.L., B.L., C.E.G., G.H., J.L.C. and L.W. generated the data, B.E.S., D.G.P., D.C.J., K.M., R.V., S. Simpson, S.Shu, J.W.C., L.B.B., M.W. and W.Y. provided materials, reagents and technical support, Z.J.C., A.S.,

A.A., Q.S., L.M.D.S., A.M.H.-K., J.L., A.M.H.-K., C.E.G., G.H., J.L.C., D.M.S., C.A.S., J.G. and J.S. analyzed the data, and Z.J.C., J.G., J.S., A.S., A.A., L.M.D.S., A.M.H.-K., D.M.S., C.A.S. and J.F.W. wrote the paper. All authors have read and approved the paper.

Competing interests

Cotton Incorporated is a not-for-profit company working with cotton scientists, the textile industry and consumers.

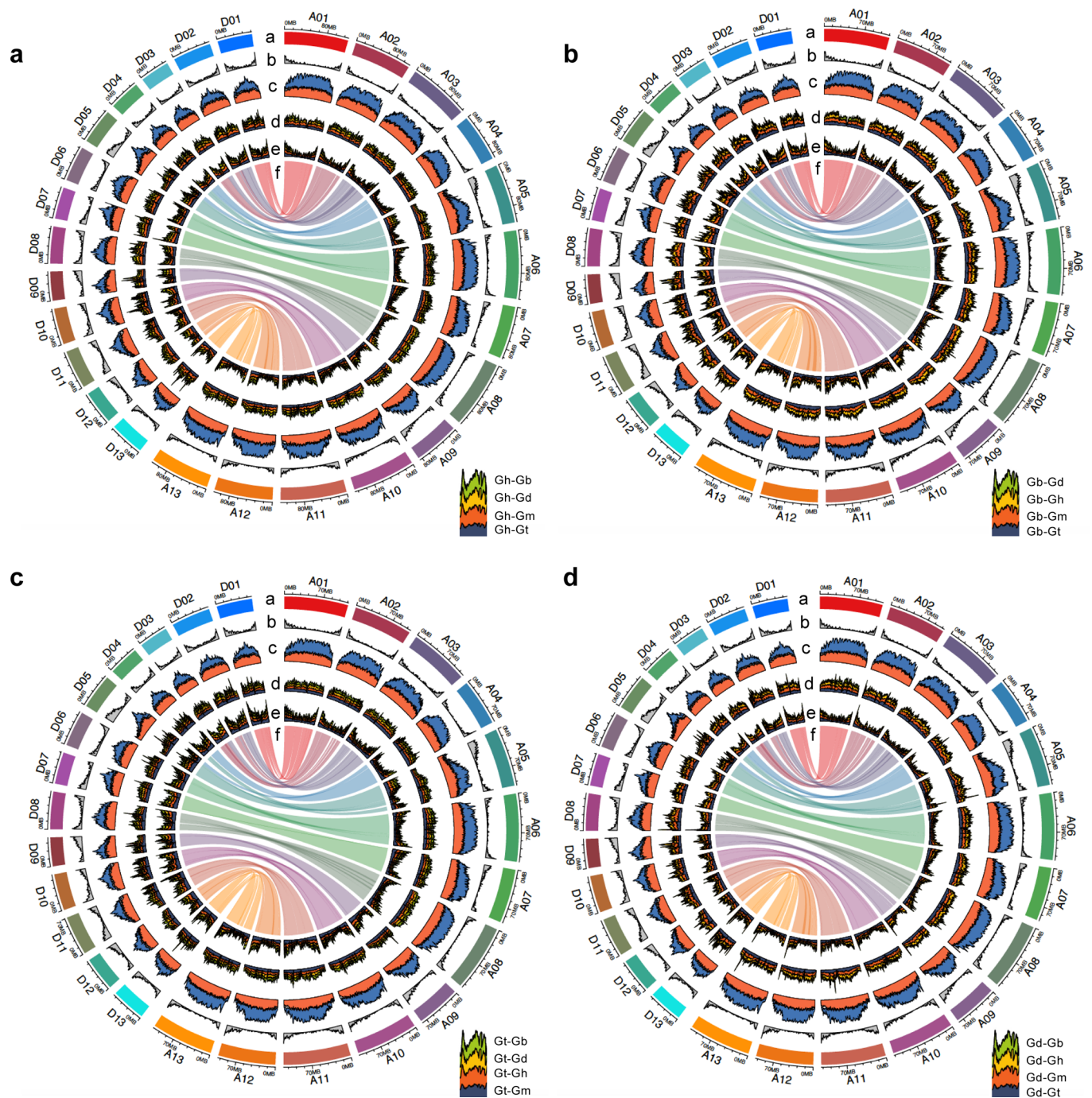
Additional information

Extended data is available for this paper at <https://doi.org/10.1038/s41588-020-0614-5>.

Supplementary information is available for this paper at <https://doi.org/10.1038/s41588-020-0614-5>.

Correspondence and requests for materials should be addressed to Z.J.C. or J.G.

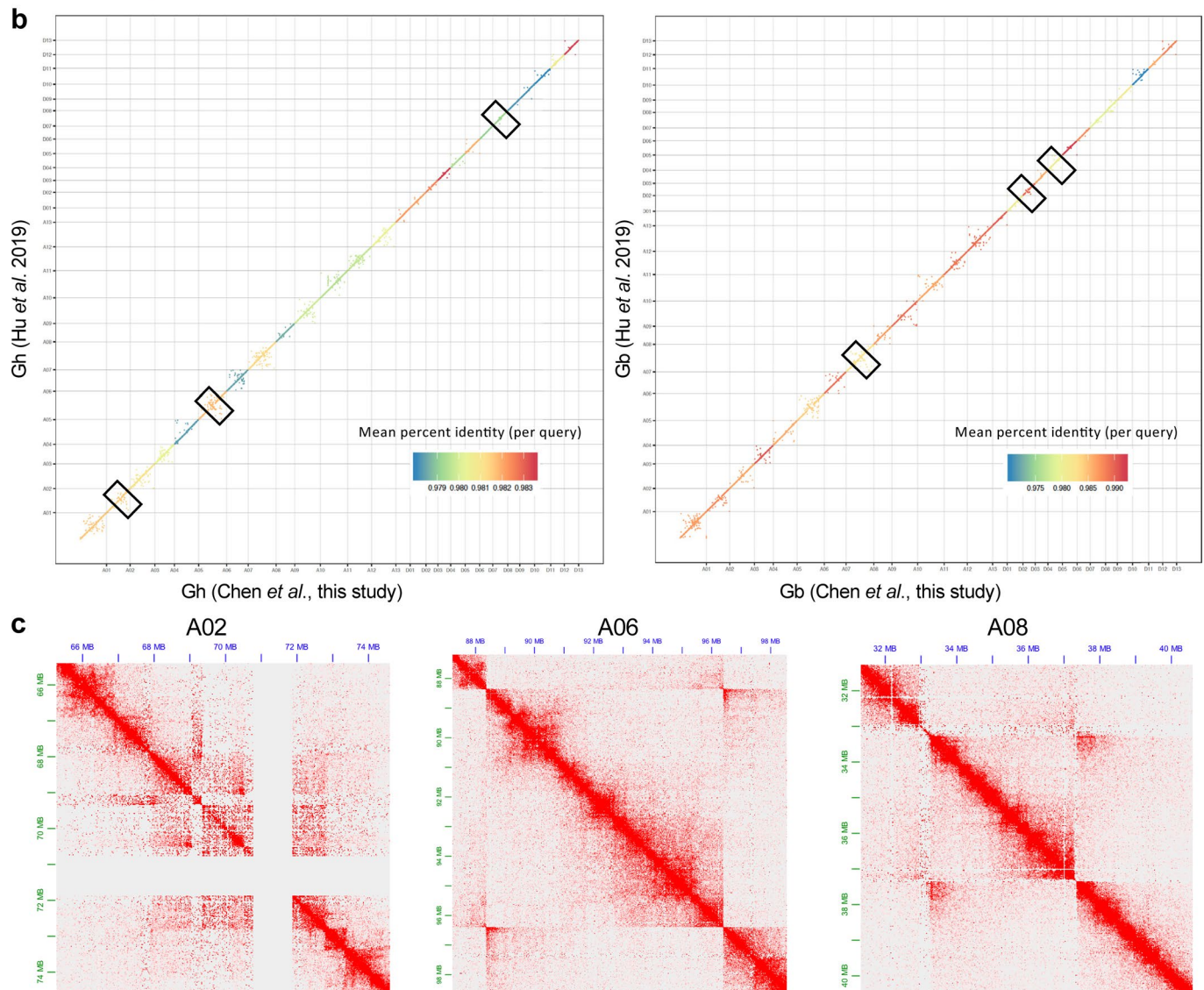
Reprints and permissions information is available at www.nature.com/reprints.



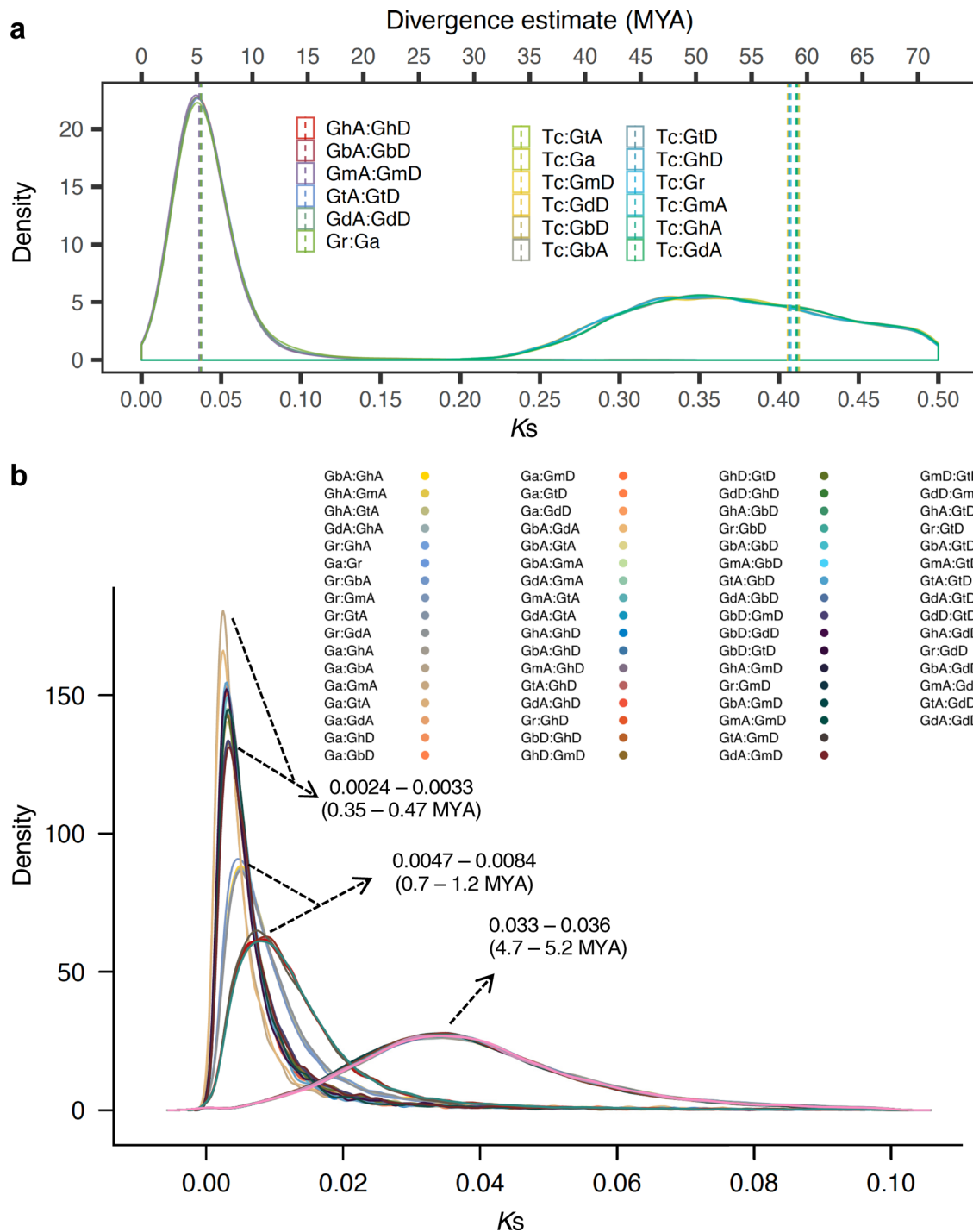
Extended Data Fig. 1 | Sequencing features of four cotton allotetraploid species. a–d, Chromosomal features and synteny of *G. hirsutum* (Gh) (a), *G. barbadense* (Gb) (b), *G. tomentosum* (Gt) (c), and *G. darwini* (Gd) (d) genomes. Notes in the circos plots: (a) estimated lengths of 13 A and 13 D homoeologous pseudo-chromosomes; (b) density distribution of annotated genes; (c) TE content (*Gypsy*, steel blue; *Copia*, grey; other repeats, orange); (d, e) stacked SNP (d) and INDEL (e) densities between species, respectively (see inset); (f) syntenic blocks between the homoeologous A and D chromosomes. The densities in plots in (b–e) are represented in 1Mb with overlapping 200-kb sliding windows.

a Summary of genome completeness assessment by 24-mer masking

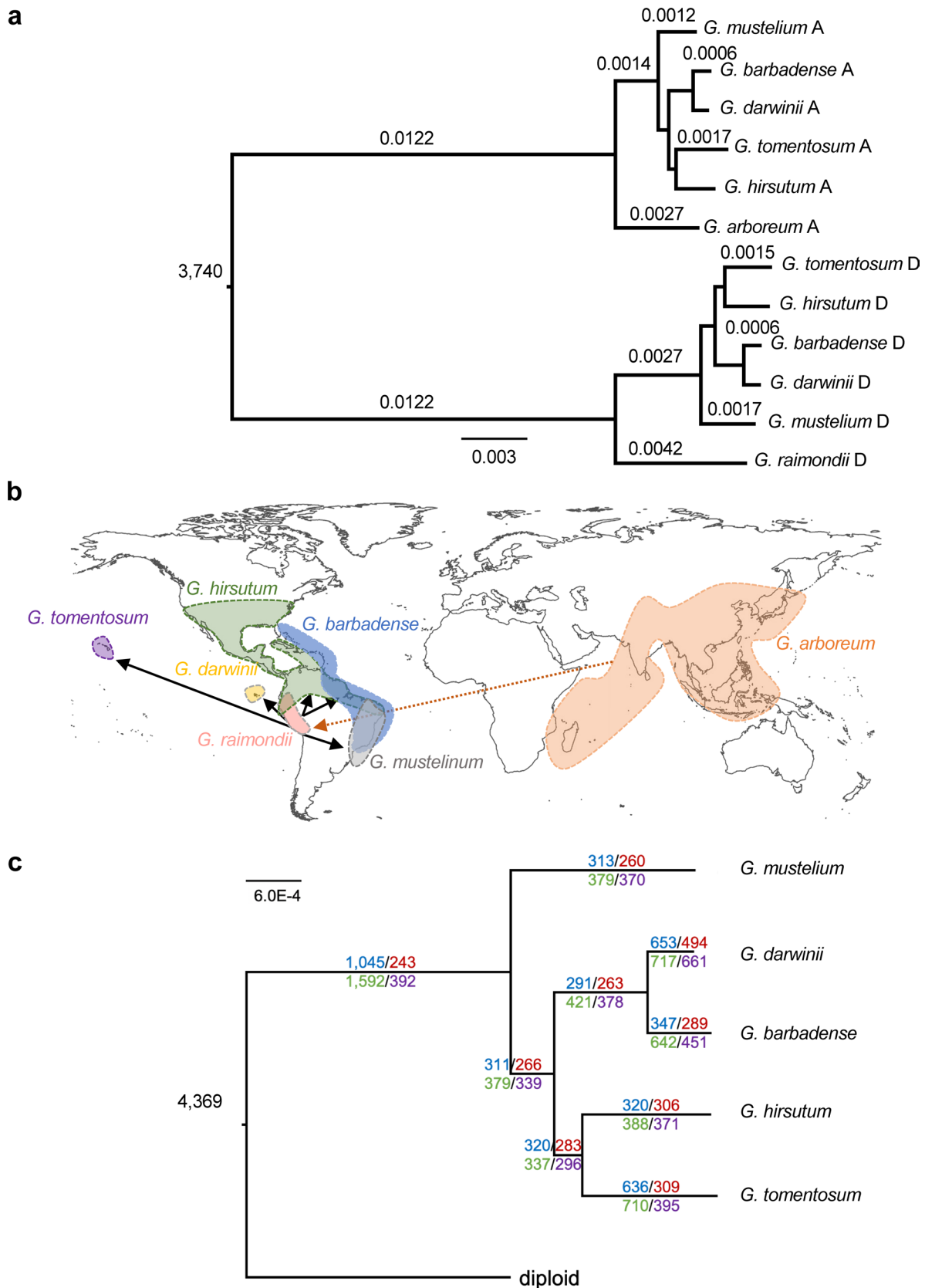
Masked Genome	Total unmasked sequences (Mb)	Total number of unmasked (>1 Kb)
Gh (Hu <i>et al.</i> 2019)	1.2	95,660
Gh (this study)	27.7	266,260
Gb (Hai7124, Hu <i>et al.</i> 2019)	3.8	90,935
Gb (3-79, this study)	10.1	24,234



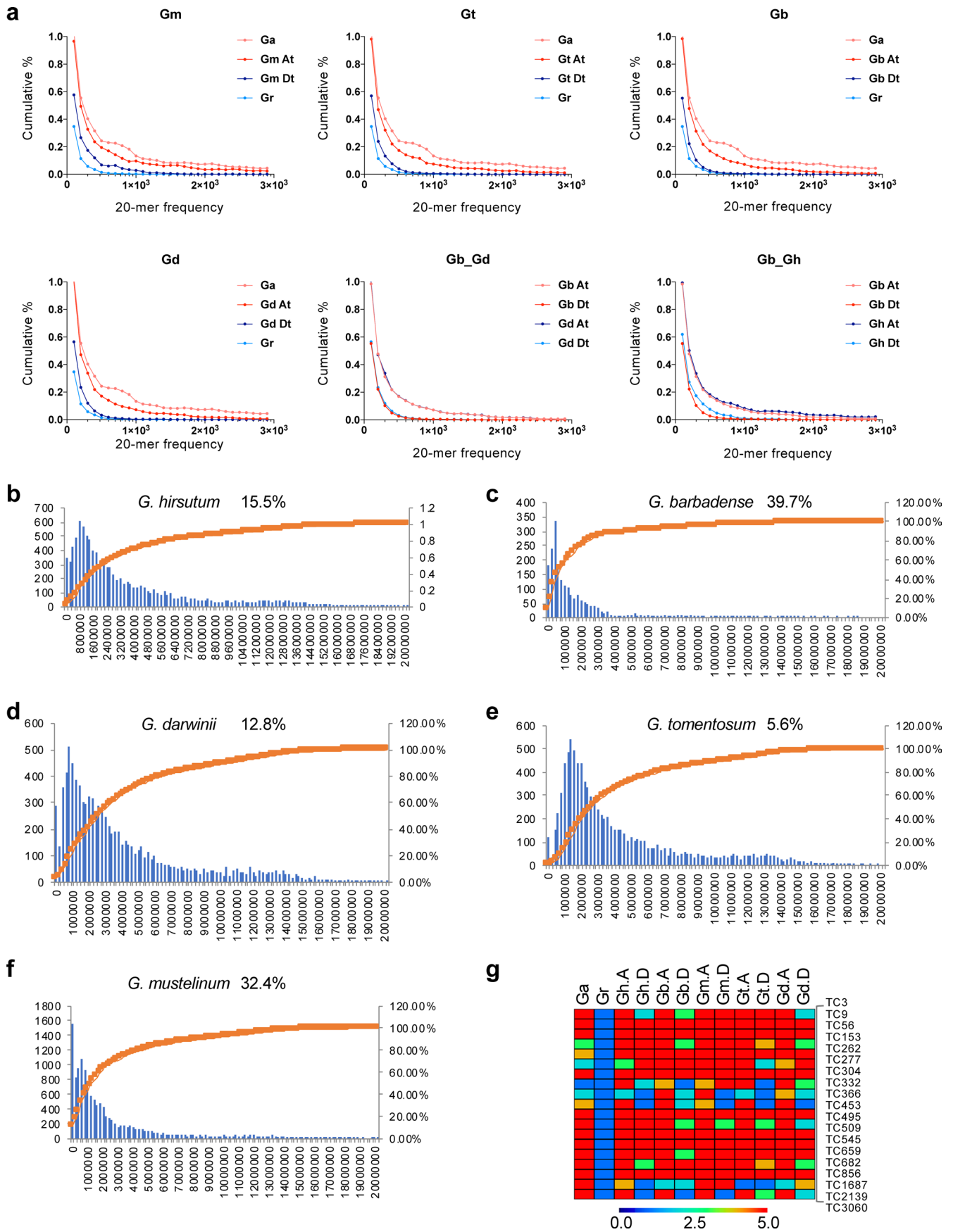
Extended Data Fig. 2 | Summary of completeness assessment and collinearity and similarity between *G. hirsutum* (Gh) and *G. barbadense* (Gb) genomes. **a, Summary of genome completeness assessment by 24-mer reciprocal masking between the published²² and our assemblies of Gh and Gb genomes. **b**, Nucleotide alignment dot plots comparing the collinearity and similarity between the genomes of Gh (published²² vs. this study, left panel) and Gb (Hai7124²² vs. 3-79 of this study, right panel). Plots show y axis (bottom to top) for chromosomes A01-A13 and D01-D13²² and x axis (left to right) for chromosomes A01-13 and D01-D13 (this study). Boxed regions represent inversions and rearrangements assessed using Hi-C data. Minimum nucleotide alignment length = 1 Kb; color scale, mean percent identity per query. **c**, Hi-C interaction maps indicating rearrangements and inversions in the published Gh genome²² with several small rearrangements flanking a large 200-Kb gap in A02, a large inversion in A06, and rearrangements in D08.**



Extended Data Fig. 3 | Estimates of divergence time based on synonymous substitution rates (K_s). **a**, The divergence time is estimated to be 58–59 million years ago (Mya) between *Theobroma cacao* and *Gossypium*. Data shown using K_s bin size of 0.001. Divergence time [$T = K_s / (2r)$] was estimated using the synonymous substitution rate (r) of 3.48×10^{-9} synonymous substitutions per synonymous site per year¹⁷ and 10,562 single copy orthologs between subgenomes and species. K_s values >1 were removed to eliminate saturated synonymous sites. **b**, The synonymous substitution rate, K_s , distribution for orthologs ($n = 21,567$), and estimates of divergence time between allotetraploid subgenomes and progenitor-like diploid genomes. Gh: *G. hirsutum*; Gb: *G. barbadense*; Ga: *G. arboreum*; Gr: *G. raimondii*; Gm: *G. mustelium*. Using a penalized-likelihood based on the concatenated nuclear tree (including branch lengths), the divergence between diploid-tetraploid clade is estimated to be 1–1.6 Mya.

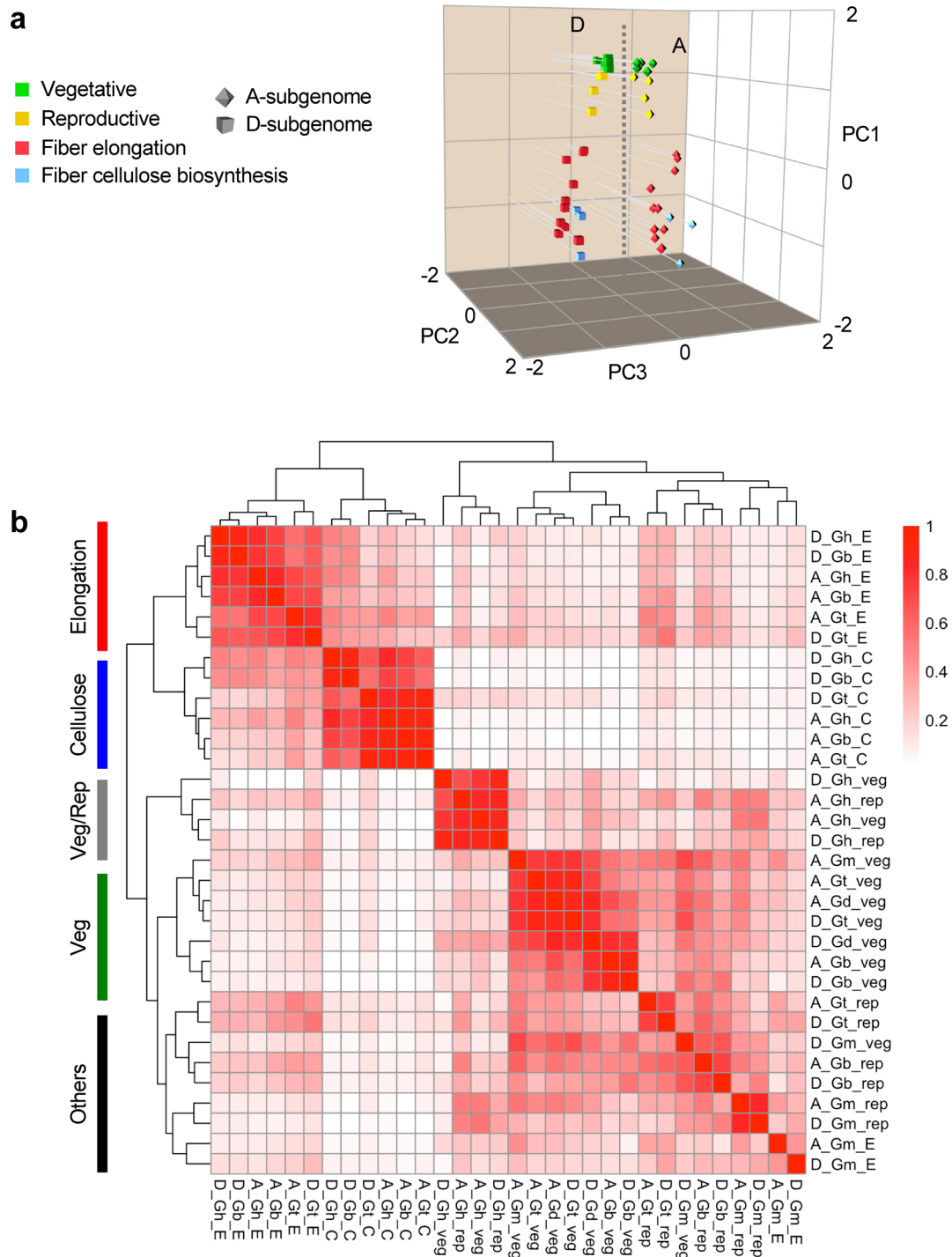


Extended Data Fig. 4 | Monophyletic origin and diversification of five allotetraploid species. **a**, The phylogeny of the polyploid species using 18,672 orthologous (37,344 homoeologous) genes and improved coalescence analysis. **b**, Geographic distribution and diversification of the five allotetraploid species *G. hirsutum*, *G. barbadense*, *G. tomentosum*, *G. darwinii*, and *G. mustelinum* and their progenitor-like diploids, *G. arboreum* and *G. raimondii*. The world map was made using R scripts, and the distribution maps were redrawn based on published maps for *Gd*, *Gt*, and *Gm*³⁰, *Gh* and *Gb*³¹, and diploid cultivated cottons³². **c**, Patterns of gene gain and loss using 4,369 single-copy orthologs (SCOs) (out of total 32,622), which are present in both diploids and in one or more allotetraploids. Numbers above and below each branch indicate number of gene gain (A-blue/D-red subgenome) or loss (A-green/D-purple subgenome), respectively.

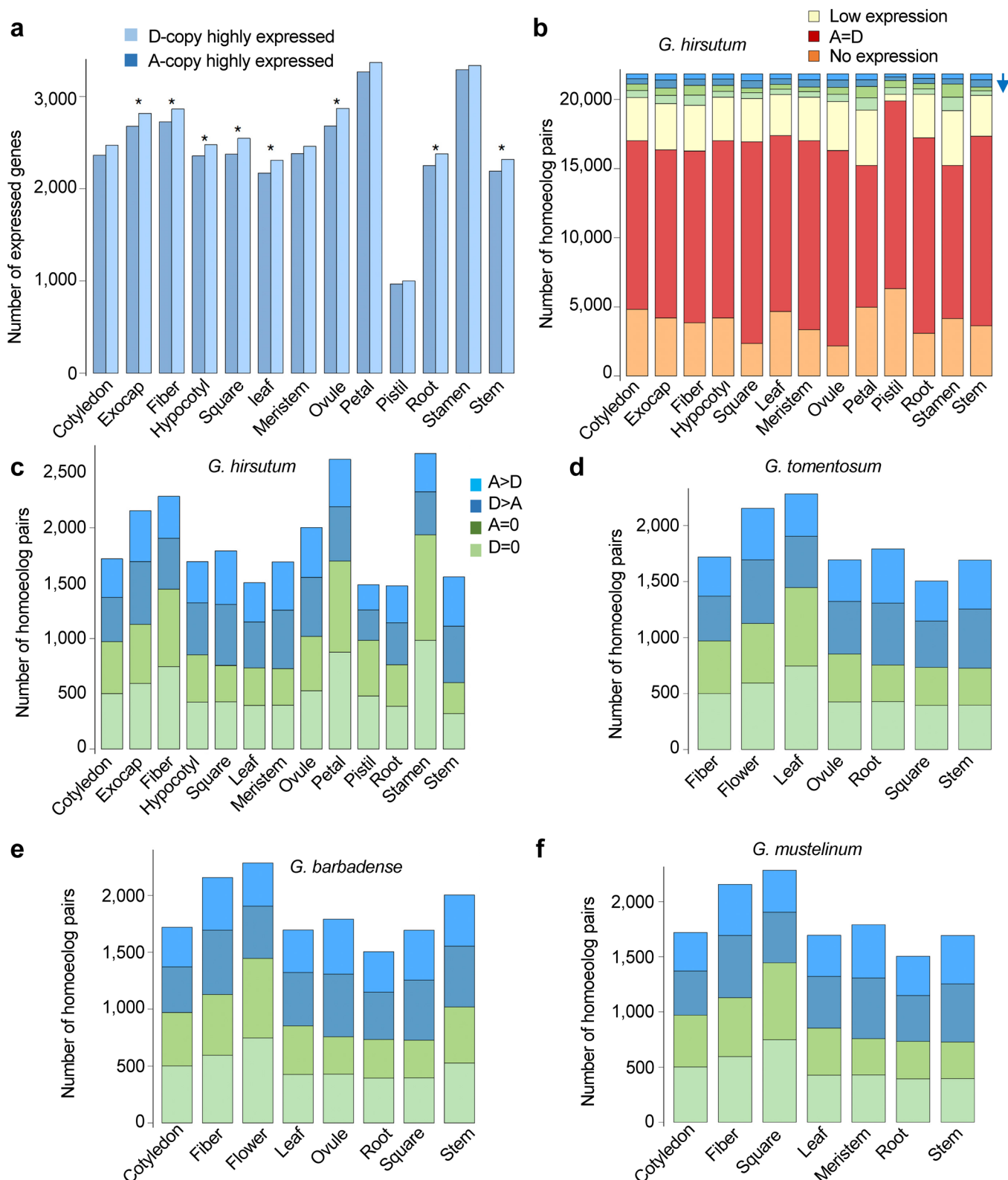


Extended Data Fig. 5 | See next page for caption.

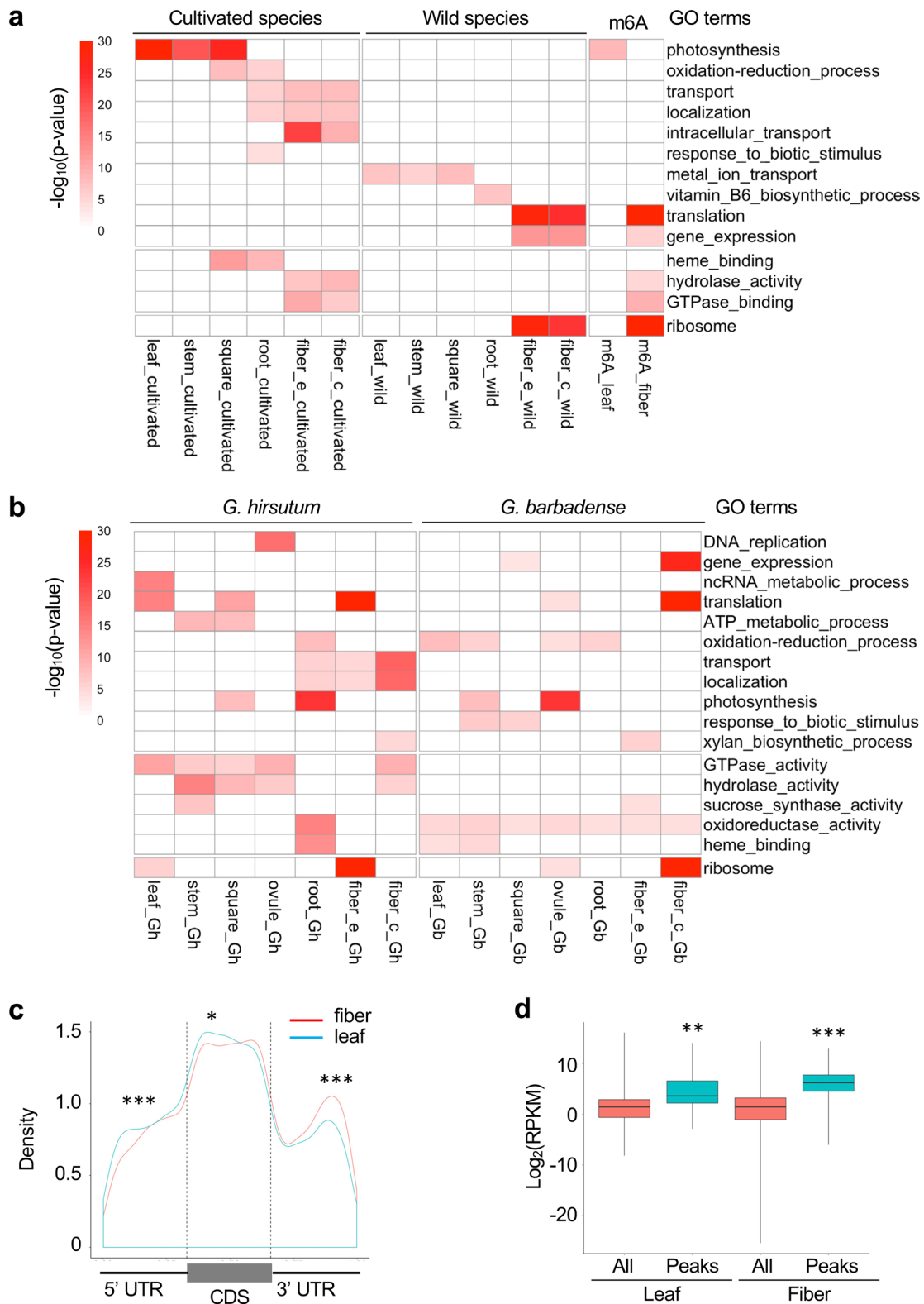
Extended Data Fig. 5 | Analysis of 20-nucleotide sequence distributions in subgenomes and *Copia* and *Gypsy* insertion time in five allotetraploid cotton species. **a**, Cumulative percentage (y axis) of 20-nucleotide sequences and their frequencies (x axis) is lower in the A subgenome than in the A (Ga) genome and higher in the D subgenome than in the D (Gr) genome in *G. mustelium* (Gm), *G. tomentosum* (Gt), *G. barbadense* (Gb), and *G. darwinii* (Gd) (from left to right). **b-f**, Number of *Copia* and *Gypsy* elements (y axis, left) relative to the estimated time of insertion (x axis) in *G. hirsutum* (**b**), *G. barbadense* (**c**), *G. darwinii* (**d**), *G. tomentosum* (**e**), and *G. mustelinum* (**f**). The right (y axis) shows cumulative % of *Copia* and *Gypsy* in the genome over divergence time (orange line). The number shown in each species indicates cumulative % of *Copia* and *Gypsy* at -600 Kya. Note: Divergence time [$T = Ks / (2r)$] was estimated using the synonymous substitution rate (r) of 3.4×10^{-9} synonymous substitutions per synonymous site per year. **g**, Movement of TEs from the A subgenomes to the D subgenomes in allotetraploids. The number of each TE cluster (TC3-TC3060, top-bottom) is shown in the right. Color scale, TE density.



Extended Data Fig. 6 | Gene expression diversity between subgenomes and among different developmental stages and five allotetraploid cotton species. a, Principal component analysis (PCA) of all genes during vegetative (leaf, stem, and root), reproductive (ovules at 0-35 DAP and square), fiber elongation (7, 14, and 21 DAP), and cellulose biosynthesis (28 and 35 DAP) stages, separating gene expression diversity among different developmental stages and between A and D subgenomes (marked by the dotted lines). **b**, Clustering analysis of 96 RNA-seq datasets with 2 biological replicates in fiber elongation (E), cellulose biosynthesis (C), vegetative (veg), and reproductive (rep) stages of cotton development.

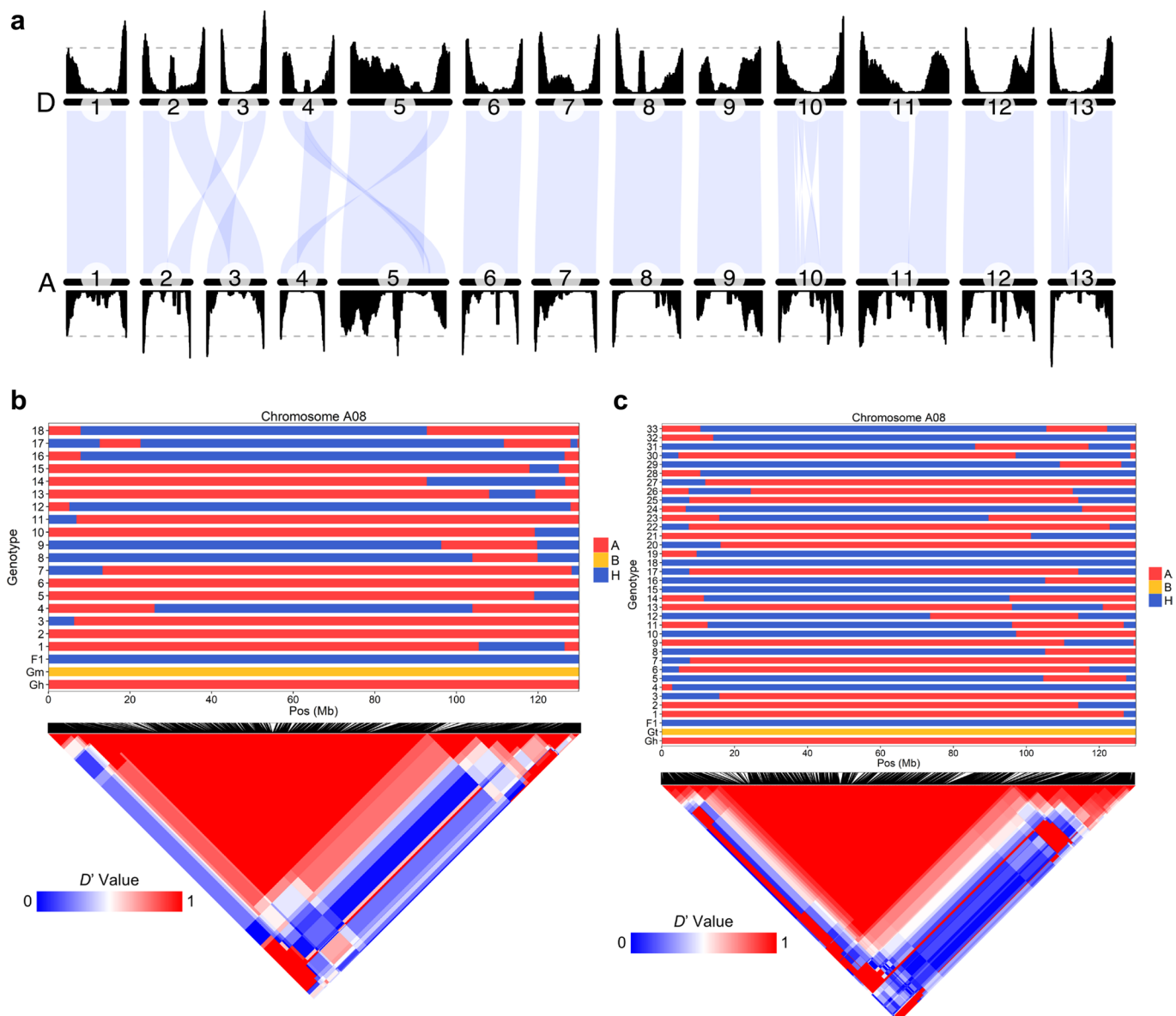


Extended Data Fig. 7 | Homeolog expression differences in four allotetraploid cotton species. **a**, Expression levels of homoeologs were compared among different tissues in each species. The number of homoeologous genes that are more highly expressed (\log_2 -fold change ≥ 1 , Benjamini-Hochberg adjusted $P < 0.05$; Wald test) in the A or D subgenome. Asterisks indicate $P < 0.05$ (two-sided binomial test). **b**, Classification of homoeologous pairs by expression patterns. The downward arrow marks the fraction that shows differential expression in different tissues of four species. **c-f**, Number of homoeolog pairs (y axis) whose expression levels are A > D (pale blue), D > A (dark blue), sub- or neo-functionalization in A (dark green) or in D (pale green) in *G. hirsutum* (**c**), *G. tomentosum* (**d**), *G. barbadense* (**e**), and *G. mustelinum* (**f**). Tissue types are shown in x axis. *G. darwinii* was not included in the analysis due to a small number of tissue types available for the study.

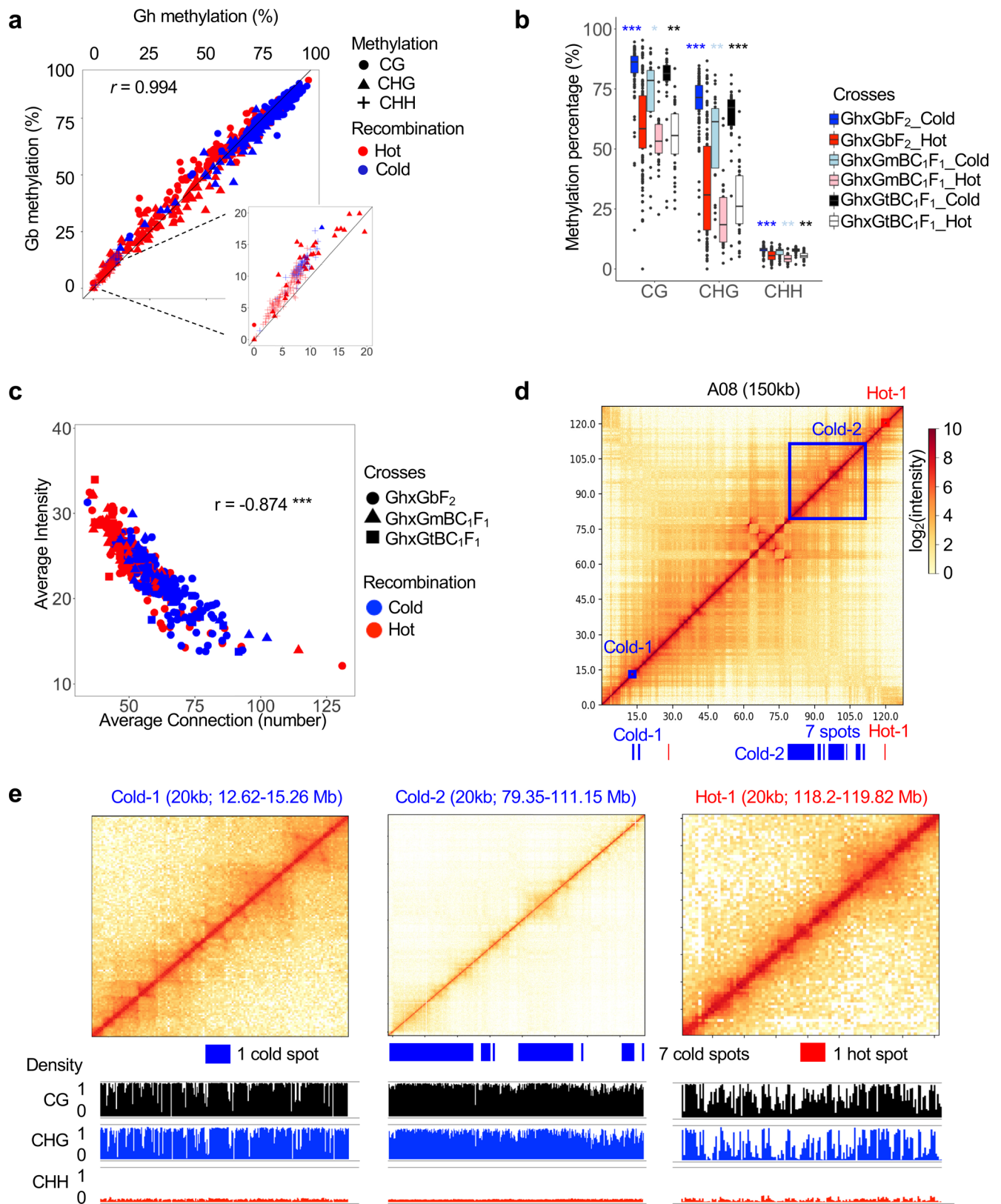


Extended Data Fig. 8 | Gene Ontology (GO) analysis of differentially expressed genes and analysis of m⁶A mRNA modifications in Upland cotton.

a, GO analysis of upregulated genes in two cultivated cottons and three wild relatives (>2-fold change, FPKM > 5, and ANOVA p-value < 0.05) and m⁶A-associated genes in the leaf and fiber of Upland cotton. Color bars = $-\log_{10}(\text{p-value})$. **b**, GO analysis of upregulated genes (>2-fold change, FPKM > 5, and ANOVA p-value < 0.05) in different tissues of *G. hirsutum* and *G. barbadense*. Color bars = $-\log_{10}(\text{p-value})$. **c**, Density of m⁶A marks in the genic region, 5' and 3' UTR of the expressed genes in the fiber (red) and leaf (green). Student's *t*-test was used to compare between m⁶A immunoprecipitated and fragmented (control) RNA reads with single (*) and triple (***) asterisks indicating statistical significance levels of $P < 0.05$ and $P < 0.001$, respectively. **d**, Expression levels (y axis) of the genes with m⁶A peaks in the leaf (161 genes) and fiber (1,205 genes) (green), relative to all homoeologous genes (red). Student's *t*-test was used to compare between m⁶A-associated genes and all homoeologous genes with double (**) and triple (***) asterisks indicating statistical significance levels of $P < 0.01$ and $P < 0.001$, respectively.



Extended Data Fig. 9 | Recombination rate distribution in *G. hirsutum* and inheritance of haplotype blocks in two breeding populations. a, Recombination rate distribution between A and D subgenomes. The recombination bins are based on overlapping 5-Mb windows. The dashed grey lines indicate 50% of individuals recombined in the window. The pale blue polygons link syntenic regions. The x axis is scaled independently for each homoeologous chromosome. **b**, Linkage disequilibrium heatmap of chromosome A08 of the *G. hirsutum*X*G. mustelinum* BC₂F₁ population. Genotypes of 18 lines each representative of one family, two parents, and F₁ are shown using the CottonSNP63K array (top panel). Red, yellow, and blue colors show the genotypes homozygous for *G. hirsutum*, homozygous for *G. mustelinum*, and heterozygous for both species, respectively. Heatmap (bottom panel) consists of equidistant tiles that indicate linkage disequilibrium as determined by a normalized coefficient of linkage disequilibrium (*D'*) between pairs of markers. Markers corresponding to SNP positions above the heatmap are congruent to the introgressed genotypes (x axis). **c**, Linkage disequilibrium heatmap of chromosome A08 of the *G. hirsutum*X*G. tomentosum* BC₃F₁ population. Genotypes of 33 lines each representative of one family, two parents, and F₁ are shown using the CottonSNP63K array (top panel). Red, yellow, and blue colors show the genotypes homozygous for *G. hirsutum*, homozygous for *G. tomentosum*, and heterozygous for both species, respectively. Heatmap (bottom panel) consists of equidistant tiles that indicate linkage disequilibrium as determined by a normalized coefficient of linkage disequilibrium (*D'*) between pairs of markers. Markers corresponding to SNP positions above the heatmap are congruent to the introgressed genotypes (x axis).



Extended Data Fig. 10 | See next page for caption.

Extended Data Fig. 10 | Correlation of DNA methylation levels and chromatin connecting sites and intensities with recombination cold (haplotype block) and hot (no block) spots. **a**, Average percentage (%) of CG (circle), CHG (triangle), and CHH (cross) methylation in the recombination hot (red) and cold (blue) spots between Gb (y axis) and Gh (x axis), with an enlarged image showing CHH methylation levels. Pearson correlation coefficient is 0.994. **b**, Average methylation percentage (y axis) of the recombination spots in different cross in CG, CHG, and CHH sites (x axis). Colors indicate recombination hot and cold spots in the three interspecific crosses GhXGbF₂ (red and blue), GmXGhBC₁F₁ (pink and light blue), and GtXGhBC₁F₁ (white and black), respectively. ANOVA was used for statistical tests with single (*), double (**), and triple (***) asterisks indicating statistical significance levels of P-value < 0.001, < 1e-5, and < 1e-10, respectively. **c**, Chromatin interaction matrices show correlation of chromatin connecting intensity (y axis, cutoff > 5) with average chromatin connecting numbers (x axis, 20-Kb window) of recombination hot (red) and cold (blue) spots in the three interspecific crosses, GhXGbF₂ (circles), GmXGhBC₁F₁ (triangles), GtXGhBC₁F₁ (squares). Pearson correlation coefficient is -0.874 with triple (***) asterisks indicating the statistical significance level of P-value < 1e-10 (Student's *t*-test). **d**, Comparison of Hi-C interaction matrix (log₂-intensity) in chromosome A08 of the GbXGhF₂ cross, consisting of recombination hot (red) and cold spots (blue). Locations for one hot spot and two cold spots are shown. **e**, Zoom-in images of two cold and one hot spots in Hi-C interaction matrix (log₂ intensity) in chromosome A08, consisting of recombination hot (red) and cold spots (blue), with CG (black), CHG (blue), and CHH (red) methylation densities (100-kb sliding windows). Values at the top of the heatmap represent Hi-C window size (20-kb) and genomic locations (Mb). Gh: *G. hirsutum*; Gb: *G. barbadense*; Gt: *G. tomentosum*; Gm: *G. mustelinum*.

Reporting Summary

Nature Research wishes to improve the reproducibility of the work that we publish. This form provides structure for consistency and transparency in reporting. For further information on Nature Research policies, see [Authors & Referees](#) and the [Editorial Policy Checklist](#).

Statistics

For all statistical analyses, confirm that the following items are present in the figure legend, table legend, main text, or Methods section.

n/a Confirmed

- The exact sample size (n) for each experimental group/condition, given as a discrete number and unit of measurement
- A statement on whether measurements were taken from distinct samples or whether the same sample was measured repeatedly
- The statistical test(s) used AND whether they are one- or two-sided
Only common tests should be described solely by name; describe more complex techniques in the Methods section.
- A description of all covariates tested
- A description of any assumptions or corrections, such as tests of normality and adjustment for multiple comparisons
- A full description of the statistical parameters including central tendency (e.g. means) or other basic estimates (e.g. regression coefficient) AND variation (e.g. standard deviation) or associated estimates of uncertainty (e.g. confidence intervals)
- For null hypothesis testing, the test statistic (e.g. F , t , r) with confidence intervals, effect sizes, degrees of freedom and P value noted
Give P values as exact values whenever suitable.
- For Bayesian analysis, information on the choice of priors and Markov chain Monte Carlo settings
- For hierarchical and complex designs, identification of the appropriate level for tests and full reporting of outcomes
- Estimates of effect sizes (e.g. Cohen's d , Pearson's r), indicating how they were calculated

Our web collection on [statistics for biologists](#) contains articles on many of the points above.

Software and code

Policy information about [availability of computer code](#)

Data collection

- (1) DNA sequencing was performed using Illumina HiSeq 2500, NovaSeq, PacBio - RSII, SEQUEL and corresponding software from the manufacturers.
- (2) RNA-seq data and m6A RNA-seq were generated using Illumina - HiSeq 2500 (2X150 bp paired-end reads) and its software.
- (3) Methylome (MethylC seq) data were generated using paired-end sequencing for 126 cycles using Illumina HiSeq 2500.
- (4) Hi-C sequencing was performed using Illumina HiSeq 2500 (2X150 bp paired-end reads), and reads were mapped using HiC-Pro.
- (5) All SNP data were generated by the CottonSNP63K Array, and genotypes were called using GenomeStudio (v2.0).

Data analysis

- (1) Assembly and annotation: We used MECAT (v1.3), QUIVER (v2.0.0), ARROW (v2.0.0), JUICER (v1.5.6) and JUICEBOX (v1.9.0) for genome assembly. Following tools were used for genome annotation: Augustus (v3.0.3); PERTRAN (v1.0); PASA (v2.3.3); InterProScan (v5.32-71.0); RepeatModeler (v1.0.11); Repeatmasker (v4.0.5); BUSCO (v2.0); EXONERATE (v2.4.0); FGENSESH+; GenomeScan (v1.0); BRAKER (v2.1.2); and BLAT (v35).
- (2) Assessment of genome completeness: We evaluated the genome assembly completeness by k-mer masking (24-mer) reciprocally between Gh (Hu et al. 2019) and Gh (this study) and between Gb (Hai 7124, Hu et al. 2019) and Gb (3-79, this study) using BBMap (v38.45). The unmasked contiguous sequences or the unshared sequence were extracted into a FASTA file and analyzed FASTA statistics. Custom Python scripts (Supplementary Dataset 19) were used for this analysis. Genome comparisons using HiC data: HiC libraries IKCF (Gh) and ILDE (Gb) were aligned to published Gh and Gb reference genomes using BWA-MEM. Heatmaps were generated using the JUICER-pre command, and visualized using JUICEBOX. Inversions and rearrangements were further identified using JUICEBOX.
- (3) Analysis of chromosomal collinearity, structural rearrangements and gene family composition between reference assemblies: Gh and Gb assemblies (Hu et al., 2019) were aligned to the assemblies generated in this study using Minimap2 with parameter setting “-ax asm5 -eqx”. The resulting alignments were used to identify structural rearrangements and local variations using SyRI. The gene copy numbers and gene families between assemblies were identified using OrthoFinder based on all annotated protein coding sequences.
- (4) Analysis of orthologs and homoeologs: We used BLAST+ (2.5.0), diamond (v0.9.21.122) and OrthoFinder (2.0) to identify

homoeologous and orthologous sequences. GO functional enrichment analysis was performed using the topGO R package (2.34.0).

(5) Evolutionary analysis: We used MUSCLE (v3.8.1551), MAFFT (v7.221 and v7.407), RAxML (v8.2.11), ASTRAL (v5.6.3), IQtree (v1.7), MACSE (v2.03), GLOOME (vMay 2013), and PAML (v4.9i) for phylogenetic analysis and evolutionary rate estimates. The evolutionary time was estimated using the formula $T = Ks/2r$, where Ks is the divergence rate, and r is the mutation rate in cotton (3.48x10⁻⁹). Rates of evolution for each subgenome of each species across the phylogeny were calculated using pairwise p-distances for the same 17,136 orthologs in all five polyploid species. The distribution of p-distances between each species was compared for both subgenomes using a one-tailed Wilcoxon Signed Rank test and Bonferroni correction for multiple testing. Differences in evolutionary rates between the subgenomes within each species were evaluated using a modified relative rate test whereby p-distance distributions were compared for both subgenomes to determine which had the greater p-distance (i.e., higher inferred rate). Differences in subgenome evolutionary rates among lineages were estimated using a modified relative rate test that again used the Wilcoxon Signed Rank test with the p-distances of 17,136 genes, here comparing p-distances between two species relative to an outgroup species. This test was repeated for all possible pairs of tip and outgroup combinations.

(6) The homeolog pairs of five species were used for estimating non-synonymous/synonymous (Ka/Ks) values. Every pair of the sequences were aligned using the MUSCLE alignment software and then transferred to the AXT format for identifying positively selected genes (PSGs, Ka/Ks>1) using the KaKs Calculator. PSGs in A and D homoeologs were compared pairwise among five species.

(7) R-gene family analysis was determined with the Hidden Markov Model (HMMER v3.2.1) and the PfamScan tool. MUSCLE v3.8.31 was used for R-gene protein alignments. R-gene statistical analysis was performed in SAS and classified with MATRIX-R.

(8) RNA-seq analysis of homoeolog expression: We used STAR (v2.5.3a) to map and count the RNA-seq reads against the reference genomes and annotations. DESeq2 (v1.14.1) was used to perform normalization and generate the expression tables and perform differential gene expression analyses. We used bwa (0.7.15-r1140) and GATK (4-4.1.2) for variant calling. Samtools (1.9), bedops (v2.4.35), and bedtools (v2.27.1) were used to operate on genomic alignment and coordinate files. For analysis across species and tissues, we used Cufflinks (v2.2.1) for expression analysis and Python (v2.7.15) and NumPy (1.16.1) for calculating ANOVA p-value and average FPKM of replicates. We also used the prcomp and cor function in R (v3.5.1) to conduct principle component analysis (PCA) and Pearson's correlation coefficient analysis, respectively. Bioconductor package topGO (v2.36.0) was used for gene ontology analysis.

(9) Co-expression network analysis was performed using WGCNA R package (1.66). Data processing was done using Python 2.7 and Python 3.6, using Biopython library (v1.70). Statistical analyses were done in R (3.5.1) using packages dplyr (0.8.0.1), data.table (1.12.0), microseq (1.2.3) and tidyverse (1.2.1). Plots were created using the R packages ggplot2 (3.1.0), ape (5.3), and ggpubr (0.2).

(10) m6ARNA-seq analysis: We used Tophat (v2.1.1) for mapping, Samtools (v1.5) for extracting uniquely mapped reads, and Bioconductor package exomePeak (v2.17.0) for identifying m6A peaks. We used intersect function of Bedtools (v2.26.0) to identify the location of RNA (5'UTR, CDS, or 3'UTR). Bioconductor package topGO (v2.36.0) was used for gene ontology analysis.

(11) K-mer and TE analyses: The LTR-harvest (function inside the genomtools 0.6.5) was used to analyze frequency and distribution of 20-mer repeat sequences in each genome. LTR-finder (v1.07) and LTR-harvest were used to identify full-length retrotransposons. LTR-retriever was used to integrate those TEs generated by both LTR-finder and LTR-harvest, as well as to predict the TE insertion time using the cotton mutation rate ($r=3.48 \times 10^{-9}$). Violin plots of insertion time were generated using ggplot2 in R.

(12) Hi-C seq and MethylC seq analyses: We used HiC-Pro (v2.11.1) for mapping and calculating interaction matrix. HiC-seq connection heatmap was generated using HiCPlotter (<https://github.com/kcakdemir/HiCPlotter>). For MethylC seq, we used Bismark (v0.18.1) for mapping and methylKit (v1.2.4) to count methylated and unmethylated cytosines. We used python (v2.7.15) for comparing average HiC-seq statistics (number of connections, intensity or interaction matrix, and distance) and DNA methylation in each recombination spots. We used prcomp function in R (v3.5.1) to calculate correlation (r or r -square values).

(13) Genotyping, haplotype and recombination rate analyses: We used BLASTn (v2.7.1+) for SNP sequence alignment and Beagle (v4.1) and PLINK (v1.90b3.45) for SNP processing. PLINK (v1.90b3.45) and HaploView (v4.2) were used for haplotype block partitioning. The statistical programming language R (v3.5.2) was used for recombination rate analysis and graphical illustrations using the R packages "MareyMap" (v1.3.4) and "ggplot2" (v3.1.0), respectively.

For manuscripts utilizing custom algorithms or software that are central to the research but not yet described in published literature, software must be made available to editors/reviewers. We strongly encourage code deposition in a community repository (e.g. GitHub). See the Nature Research [guidelines for submitting code & software](#) for further information.

Data

Policy information about [availability of data](#)

All manuscripts must include a [data availability statement](#). This statement should provide the following information, where applicable:

- Accession codes, unique identifiers, or web links for publicly available datasets
- A list of figures that have associated raw data
- A description of any restrictions on data availability

SUBID BioProject BioSample Accession Organism

SUB5895679 PRJNA516411 SAMN10992405 VKDL00000000 Gossypium barbadense
 SUB5895750 PRJNA516409 SAMN10884649 VKGI00000000 Gossypium darwinii
 SUB5899309 PRJNA515894 SAMN11351207 VKGJ00000000 Gossypium hirsutum
 SUB5899582 PRJNA516412 SAMN11289623 VKGE00000000 Gossypium tomentosum
 SUB5901069 PRJNA525892 SAMN11110849 VKGF00000000 Gossypium mustelinum

Note: Assemblies are still in manual review and will be released under those accession numbers.

All other datasets were deposited in GenBank or GEO with accession numbers or shown in Supplemental Datasets or Tables.

Field-specific reporting

Please select the one below that is the best fit for your research. If you are not sure, read the appropriate sections before making your selection.

Life sciences Behavioural & social sciences Ecological, evolutionary & environmental sciences

For a reference copy of the document with all sections, see [nature.com/documents/nr-reporting-summary-flat.pdf](https://www.nature.com/documents/nr-reporting-summary-flat.pdf)

Life sciences study design

All studies must disclose on these points even when the disclosure is negative.

Sample size	<p>Sample size per group or condition was determined based on the minimum number of biological replicates required to perform differential expression analysis as per software tools used and previously published literature.</p> <p>Sample size for linkage map analysis was determined based on the minimum number of individuals required to generate a linkage map. The number of cultivars included in the diversity panel was based on data availability and analytical sufficiency.</p>
Data exclusions	<p>Samples were excluded if they failed at the library preparation stage or those that displayed poor correlation between biological replicates.</p> <p>SNPs were excluded if they did not meet the minimum BLASTn parameters for sequence alignment. A SNP was excluded if there was mapping ambiguity between the reference genome and the linkage mapping populations. This was done to reduce the occurrence of erroneous alignments that may result due to repetitive and homeologous sequences within the JGI G. hirsutum v2 reference genome.</p>
Replication	<p>Findings were consistent between biological replicates and different sequencing plates/batches.</p> <p>Linkage mapping populations were not replicated due to resource constraints.</p>
Randomization	<p>Order of sample processing for library preparation and sequencing were processed in multiple batches as and when they were received from collaborating laboratories, kind of randomization in itself, but following stringent standardized protocols.</p> <p>Linkage mapping software randomizes starting order of SNP markers across multiple iterations to determine optimal starting order. Randomization does not affect haplotype partitioning and thus was not used in the cultivar analysis.</p>
Blinding	<p>No blinding took place. To alleviate any complications from non-blinded analyses all samples were analyzed simultaneously in the same manner regardless of their condition/origin.</p> <p>All specimens' identities were encoded before submission for genotyping.</p>

Reporting for specific materials, systems and methods

We require information from authors about some types of materials, experimental systems and methods used in many studies. Here, indicate whether each material, system or method listed is relevant to your study. If you are not sure if a list item applies to your research, read the appropriate section before selecting a response.

Materials & experimental systems

n/a	Involved in the study
<input type="checkbox"/>	<input checked="" type="checkbox"/> Antibodies
<input checked="" type="checkbox"/>	<input type="checkbox"/> Eukaryotic cell lines
<input checked="" type="checkbox"/>	<input type="checkbox"/> Palaeontology
<input checked="" type="checkbox"/>	<input type="checkbox"/> Animals and other organisms
<input checked="" type="checkbox"/>	<input type="checkbox"/> Human research participants
<input checked="" type="checkbox"/>	<input type="checkbox"/> Clinical data

Methods

n/a	Involved in the study
<input checked="" type="checkbox"/>	<input type="checkbox"/> ChIP-seq
<input checked="" type="checkbox"/>	<input type="checkbox"/> Flow cytometry
<input checked="" type="checkbox"/>	<input type="checkbox"/> MRI-based neuroimaging

Antibodies

Antibodies used	Affinity purified anti-m6A rabbit polyclonal antibody (Synaptic Systems, cat. no. 202 003)
Validation	Information of Affinity purified anti-m6A rabbit polyclonal antibody (https://www.sysy.com/factsheets/202_003.pdf).